Published in final edited form as:
Nat Biotechnol. 2021 April 01; 39(4): 510–519. doi:10.1038/s41587-020-0742-6.

A comprehensive library of human transcription factors for cell fate engineering

Alex H.M. Ng[1,2,3,*], **Parastoo Khoshakhlagh**[1,2,3,*], **Jesus Eduardo Rojo Arias**[4,5], **Giovanni Pasquini**[4], **Kai Wang**[6,7], **Anka Swiersy**[4], **Seth L. Shipman**[8], **Evan Appleton**[1,2,3], **Kiavash Kiaee**[1,2,3], **Richie E. Kohman**[1,2], **Andyna Vernet**[2], **Matthew Dysart**[1,2], **Kathleen Leeper**[1,2], **Wren Saylor**[1,2], **Jeremy Y. Huang**[1,2], **Amanda Graveline**[2], **Jussi Taipale**[9,10,11], **David E. Hill**[1,12], **Marc Vidal**[1,12], **Juan M. Melero-Martin**[6,7], **Volker Busskamp**[4,13,^], **George M. Church**[1,2,3,^]

[1]Department of Genetics, Blavatnik Institute, Harvard Medical School, Boston MA, 02115, USA [2]Wyss Institute for Biologically Inspired Engineering at Harvard University, Boston, MA, 02115, USA [3]GC Therapeutics, Inc., Cambridge, MA, 02139, USA [4]Technische Universität Dresden, Center for Molecular and Cellular Bioengineering (CMCB), Center for Regenerative Therapies Dresden (CRTD), Dresden, 01307, Germany [5]Wellcome-MRC Cambridge Stem Cell Institute, Jeffrey Cheah Biomedical Centre, Cambridge Biomedical Campus, University of Cambridge, Cambridge, UK [6]Department of Cardiac Surgery, Boston Children's Hospital, Boston, MA 02115, USA [7]Department of Surgery, Harvard Medical School, Boston, MA 02115, USA [8]Gladstone Institutes and University of California, San Francisco, San Francisco, CA, 94158, USA [9]Department of Biochemistry, University of Cambridge, UK [10]Department of Medical Biochemistry and Biophysics, Karolinska Institute, Stockholm, Sweden [11]Applied Tumor Genomics Program, Faculty of Medicine, University of Helsinki, Helsinki, Finland [12]Center for Cancer Systems Biology (CCSB), Dana-Farber Cancer Institute, Boston, MA, 02215, USA [13]Department of Ophthalmology, Medical Faculty, University of Bonn, Bonn, 53127, Germany

Abstract

Human pluripotent stem cells (hPSCs) offer an unprecedented opportunity to model diverse cell types and tissues. To enable systematic exploration of the programming landscape mediated by

^Corresponding authors. gchurch@genetics.med.harvard.edu or volker.busskamp@ukbonn.de.
*Co-first authors.

Author contributions.
A.H.M.N., P.K., V.B. and G.M.C. conceived the idea, led the study, and designed all experiments. A.H.M.N. and P.K. performed the majority of the experiments and analyses, with significant technical contribution from J.E.R.A, G.P., K.W., A.S., S.L.S., E.A., K.K., R.E.K., A.V., M.D., K.L., W.S., J.Y.H., A.G., J.T., D.E.H., M.V. and J.M.M.-M. V.B. and G.M.C. oversaw the study. A.H.M.N., P.K. and V.B. wrote the manuscript with input and feedback from all authors.

Competing interests.
A.H.M.N., P.K., V.B., and G.M.C. are inventors on patents filed by the Presidents and Fellows of Harvard College. Full disclosure of G.M.C. is available on http://arep.med.harvard.edu/gmc/tech.html. A.H.M.N., P.K. and G.M.C. are co-founders and have equity in GC Therapeutics, Inc. No reagents or funding from GC Therapeutics, Inc. was used in this study.

Materials & Correspondence.
Requests should be addressed to gchurch@genetics.med.harvard.edu or volker.busskamp@ukbonn.de.

Europe PMC Funders Author Manuscripts

transcription factors (TFs), we present the Human TFome, a comprehensive library containing 1,564 TF genes and 1,732 TF splice-isoforms. By screening the library in three hPSC lines, we discovered 290 TFs, including 241 previously unreported, that induce differentiation in four days without alteration of external soluble or biomechanical cues. We used four of the hits to program hPSCs into neurons, fibroblasts, oligodendrocytes and vascular endothelial–like cells that have molecular and functional similarity to primary cells. Our cell-autonomous approach enabled parallel programming of hPSCs into multiple cell types simultaneously. We also demonstrated orthogonal programming by including oligodendrocyte-inducible hPSCs with unmodified hPSCs to generate cerebral organoids, which expedited *in situ* myelination. Large-scale combinatorial screening of the Human TFome will complement other strategies for cell engineering based on developmental biology and computational systems biology.

Introduction

A longstanding goal of stem cell, tissue and organoid engineering is the creation of any cell type or tissue in a facile, controlled manner. This is foundational for accurate cellular modeling in fundamental science, disease modeling, drug discovery and regenerative medicine. hPSCs have a virtually unlimited expansion capability and the potential to differentiate into any cell type. However, reliable protocols to generate most cell lineages are lacking, and existing protocols are often limited by long timescales or modest efficiencies. Many established protocols attempt to mimic the complexity of developmental biology, with its protracted timelines. During development, the process of cell type specification is intertwined with other regulatory events that spatiotemporally position the proper cell types in defined population sizes, but are not relevant to *in vitro* protocols that aim to rapidly generate the largest number of cells. Most current protocols also depend on external signals with known roles in development, such as soluble factors or mechanical cues, which converge on TFs to control cell type–specific genetic programs. This reliance on external cues, which are often incompatible between different specialized cell types, makes it challenging to generate multiple lineages in the same culture.

An alternative approach is direct activation of TFs, which can both shorten the time for cell conversion and isolate it from other developmental events. TF induction has been shown to transdifferentiate cells between lineages[1], reprogram somatic cells to pluripotency[2], and differentiate stem cells[3]. Previous studies on applying TFs for cell fate engineering have used either experimental testing of a limited set of developmentally relevant TFs[4–8] or computational prediction of TFs inferred from genome-scale datasets with modest accuracy[9–11]. However, the field has lacked a global experimental study of the estimated 1,600 TFs in the human genome[12]. The largest screen to our knowledge explored 481 TFs at once[13].

After constructing the Human TFome, we screened each TF for its ability to induce differentiation of three human induced pluripotent stem cell (hiPSC) lines. Of the 290 hits, we found that 241 had not been previously associated with cell differentiation. We characterized four of the 290 TFs in depth — *ATOH1, NKX3-1, ETV2* and *SOX9* — which programmed hiPSCs within four days into induced neurons, induced fibroblasts, vascular

endothelial–like cells and induced oligodendrocytes, respectively. We also demonstrated parallel programming of hiPSCs into two or three defined cell types simultaneously in the same culture without lineage-specific cues. Finally, we developed an orthogonal programming approach by including *SOX9*-engineered, oligodendrocyte-producing hiPSCs at the genesis of developmentally inspired cerebral organoids, which accelerated myelination.

Results

290 transcription factors individually induce stem cell differentiation

We generated a library containing 1,564 human TFs, including 1,732 splice-isoform-level open reading frames (ORFs) (Supplementary Fig. 1a,b and Supplementary Table 1; Methods), annotated based on a rigorous curation[14]. Cloning from cDNA is a bottleneck in generating ORF collections owing to low or tissue-confined TF expression in the source material. We overcame this by de novo synthesis of the 273 ORFs that were not available in existing large ORF collections[15–18] (Supplementary Fig. 1c) and merged them to create the Human TFome.

To express the Human TFome in hiPSCs, we first cloned the library as one pool into an all-in-one doxycycline-inducible (Tet-On), puromycin-selectable lentiviral vector (Supplementary Fig. 1d-h). We ensured that cells received at most one TF by transducing them with the pooled library at a low multiplicity of infection (MOI of 0.1), and we confirmed the induction of TF overexpression (Supplementary Fig. 1i). We transduced in triplicates three hiPSC lines (PGP1, CRTD5 and ATCC-DYS0100) that have similar characteristics (i.e., all reprogrammed from male fibroblasts using Sendai virus) to reduce effects arising from the variability between hiPSC lines. Greater than 87% TF coverage was achieved in all three hiPSC lines (Supplementary Fig. 1j) by transducing a sufficient number of cells.

We used loss of pluripotency as a readout and enriched two cell populations by fluorescence-activated cell sorting (FACS): (i) ‘differentiated’ cells, which we define here as cells that have down-regulated expression of pluripotency markers but have not been evaluated for expression of cell type–specific markers, and (ii) cells that remained pluripotent (Fig. 1a, Supplementary Fig. 2a). Four days post TF induction (dpi), we stained cells for the pluripotency marker TRA-1-60[19,20] and sorted for differentiated cells (low TRA-1-60 signal) and pluripotent cells (high TRA-1-60 signal) (Supplementary Fig. 2b,c). To identify TFs enriched in the two populations, we amplified the integrated TFs using universal primers for Illumina sequencing and sequenced them. A score threshold defined by the ratio of TF counts in TRA-1-60 low versus high gates was used to identify TFs responsible for differentiation (Supplementary Fig. 2d, see Methods).

Our screen identified 290 TFs that individually induced differentiation in at least two hiPSC lines and 65 TFs in all three lines (Fig. 1b, Supplementary Fig. 2e, Supplementary Table 2, 3), despite the variability between hiPSC lines[21, 22]. A PubMed query indicated that 241 of the 290 TFs (83.1%) and 54 of the 65 TFs (83.0%) have not been previously reported as programming or differentiation factors upon overexpression (Fig. 1b, Supplementary Table

4). The hits included known differentiation-inducing TFs, such as *NEUROG1* [20] and *ASCL1* [23], confirming the biological relevance of our screen. For validation, we selected the top TFs in each of the four overlapping groups of hits from the three lines (Supplementary Fig. 2e), for a total of 16 TFs. For screening, we used lentiviruses owing to their highly titratable transduction, which enabled us to perform a controlled Human TFome screen at a single copy per cell. However, to validate individual TFs, we used PiggyBac transposons, both to avoid the multi-step lentiviral production, which impedes high-throughput cell line engineering, and to reduce the silencing and variable expression associated with lentiviral vectors. Indeed, we observed increased differentiation efficiency using PiggyBac compared to lentivirus for a positive-control TF, *NEUROG1* (Fig. 1c). All 16 TFs were successfully validated in the PiggyBac system based on the loss of *NANOG, OCT4/POU5F1* or *SOX2* expression at 4 dpi (Fig. 1d, Supplementary Fig. 2f).

Next, we characterized the identity and functionality of the differentiated cells induced by four TFs: *ATOH1, NKX3-1, ETV2* and *SOX9*.

ATOH1 programs hiPSCs into induced neurons

ATOH1 was the most efficient driver of differentiation in all three hiPSC lines (Fig. 1d). This TF has been implicated in the development of inner ear hair cells[24]. It has also been used to induce neuronal differentiation in stem cells in conjunction with soluble neurogenesis cues and culturing techniques[25,26]. We tested whether ATOH1 alone is sufficient to program hiPSCs into induced neurons without specialized culturing conditions. Indeed, we observed rapid four-day neuronal programming without changing the media composition, as 99±1% of *ATOH1*-induced cells were positive for the neuronal marker *NCAM* (Fig. 2a), and cells exhibited neuronal morphology based on *TUBB3* (Fig. 2b) and *NF200* protein expression (Supplementary Fig. 3a). *ATOH1*-programmed cells and primary neurons were transcriptomically similar based on unbiased principal component analysis (PCA) (Fig. 2c) and up-regulation of key neuronal genes (Fig. 2d, Supplementary Table 5). This was corroborated by CellNet network-based transcriptomic analysis (Supplementary Fig. 3b) and by the enrichment of neuronal gene ontologies in the up-regulated genes (Supplementary Fig. 3c). Furthermore, the down-regulation of pluripotency genes was confirmed transcriptionally (Supplementary Fig. 3d). We categorized these cells as ‘induced,’ which we define here as cells with concurrent expression of functional markers of a specific lineage and residual levels of pluripotency markers.

To assess the function of the induced neurons, after 4 dpi, we cultured them without further doxycycline administration in neuronal maturation media and performed whole-cell patch-clamp electrophysiology. We observed single action potentials in response to current injection at 7 dpi (Supplementary Fig. 3e), trains of action potentials at 14 dpi (Fig. 2e) and spontaneous action potentials at 21 dpi (Supplementary Fig. 3f, summarized in Fig. 2f). Altogether, these results show that ATOH1 alone can program hiPSCs into induced neurons that remain functional in long-term cultures.

NKX3-1 programs hiPSCs into induced fibroblasts

NKX3-1 was the second most efficient hit from our validation studies (Fig. 1d). This TF is essential in prostate differentiation[27] and can replace *OCT4/POU5F1* in fibroblast reprogramming into iPSCs[28]. However, *NKX3-1* has not been reported for hPSC differentiation. We used CellNet[29] to ascertain the identity of *NKX3-1* induced cells based on transcriptomic network analysis: *NKX3-1*-programmed cells were serendipitously identified as fibroblasts (Supplementary Fig. 4a).

We overexpressed *NKX3-1* in hiPSCs with no additional soluble differentiation cues. At 4 dpi, 79±2% of the cells expressed the fibroblast marker *VIM* as revealed by flow cytometry (Fig. 2g, Supplementary Fig. 4b). *NKX3-1*-induced cells were also positive for *ALCAM* and *HSP47* by immunostaining (Fig. 2h). The cells had a transcriptomic signature similar to that of primary fibroblasts based on unbiased PCA (Fig. 2i) and up-regulation of key fibroblast genes as shown by RNA-seq (Fig. 2j, Supplementary Table 5). Gene ontology analysis showed up-regulation of fibroblast-associated genes (Supplementary Fig. 4c) and down-regulation of the pluripotency genes *NANOG, OCT4/POU5F1* and *SOX2* (Supplementary Fig. 4d).

A hallmark of fibroblasts is their function in wound healing and their ability to remodel the extracellular matrix. These can be assessed in scratch[30] and collagen contraction assays[31] *in vitro*. At 4 dpi, without switching to fibroblast-specific media and without further doxycycline administration, after we scratched the monolayer of *NKX3-1*-induced cells, the cells migrated to seal the wound, whereas uninduced cells did not (Fig. 2k,l). In a separate functional assay, collagen-embedded NKX3-1-induced cells were able to contract and reduce the surface area of the collagen gel (Supplementary Fig. 4e,f). Hence, our data demonstrated that *NKX3-1* alone is a potent driver of differentiation into induced fibroblasts, with functionality *in vitro*.

ETV2 isoform 2 programs hiPSCs into vascular endothelial–like cells

Our differentiation approach, which does not use lineage-specific media, may facilitate the generation of multiple cell types in the same culture. Given the importance of vascularization in building synthetic tissues, along with the indispensable role of ETV2 in vascular differentiation from PSCs32, we aimed to determine *ETV2*'s programming ability without lineage-specific media. We queried *ETV2*'s rank in our screen, where it was among the top hits in one of the three hiPSC lines. As TF splice-isoforms play important roles in cell differentiation[33] and only *ETV2* isoform 1 was included in the screen, we aimed to determine the impact of all four of ETV2's annotated splice-isoforms (Supplementary Fig. 5a) on cell-autonomous vascular cell conversion. The ETV2 isoform used in a previous study for hiPSC differentiation[32] could not be readily ascertained, and the contribution of these isoforms to vascular programming without lineage-specific media has not been examined.

We tested all four isoforms of *ETV2* independently and found that isoforms can have a major impact on programming efficiency. Using *ETV2* isoform 2 (ENST00000402764.6), 95±0.2% of cells expressed the endothelial cell marker VE-Cadherin (*CDH5*) (Fig. 3a),

compared with only 48±1% using the longer *ETV2* isoform 1 (Fig. 3a). The other two isoforms had low to no ability to induce endothelial conversion (isoform 3: 21±2% and isoform 4: 0±0%, Fig. 3a), despite similar integrated vector copy numbers for all four isoforms (Supplementary Fig. 5b). Only isoform 2 induced nearly complete expression of VE-Cadherin, with its characteristic cobblestone morphology (Fig. 3b). We examined the functionality of these four cell populations in angiogenesis assays. Only isoform 2 had high tubulogenesis capability (Fig. 3c).

We focused on *ETV2* isoform 2, the most potent splice variant, for deeper analysis. These cells had a transcriptomic signature similar to that of primary endothelial cells based on unbiased PCA (Fig. 3d), up-regulation of key vascular endothelial genes (Fig. 3e, Supplementary Table 5) and a transcriptomic comparison of highly variable genes (Supplementary Fig. 5c). They also had an endothelial cell type classification based on CellNet network-based transcriptomic analysis (Supplementary Fig. 5d) and on endothelial gene ontology analysis of the up-regulated genes (Supplementary Fig. 5e). Furthermore, we detected increased expression of *PLVAP, PECAM1* and *CDH5* (VE-Cadherin) in *ETV2*-isoform-2-induced cells, along with down-regulation of pluripotency genes by single cell RNA-seq (scRNA-seq) (Fig. 3f). Down-regulation of pluripotency genes was further confirmed by bulk RNA-seq (Supplementary Fig. 5f) and flow cytometry (Supplementary Fig. 5g). While these cells expressed endothelial functional markers, they continued to express residual amounts of the pluripotency marker OCT4 at day 4. We therefore defined them as ‘vascular endothelial-like’ cells. Notably, the cells remained stably programmed after the induction of exogenous *ETV2* isoform 2 was stopped (Supplementary Fig. 5h).

We assessed the angiogenic ability of the cells. Using an *in vitro* tube formation assay, we observed lumens by transmission electron microscopy (TEM) (Fig. 3g) with diameters of 4.3±0.7μm (Fig. 3h) and tight junctions (Supplementary Fig. 5i), similar to that of capillaries *in vivo* [34]. To assess function in vivo, we transplanted *ETV2*-induced cells subcutaneously into nude mice. Seven days post transplantation, we observed mature blood vessels derived from the cells, as evidenced by human-specific CD31-lined lumens supported by mouse SMA-positive perivascular cells (Fig. 3i). The blood vessels integrated with the host circulatory system and were perfused, as shown by the presence of host red blood cells within their lumens in a serial tissue section (Fig. 3j). We observed 40±6 vessels/mm^2 on average (Fig. 3k).

Parallel cell programming in co-cultures

With the aim of constructing complex tissues, we investigated the concept of parallel programming. In this approach, multiple lineages are generated simultaneously in the same dish in lineage-independent media (Fig. 4a). We mixed inducible neuronal, endothelial and fibroblast hiPSCs in a pairwise fashion with identical ratios (i.e. *ETV2+NKX3-1, ATOH1+NKX3-1* and *ATOH1+ETV2* hiPSCs) and activated TF expression for four days. The final cell populations were assessed by immunostaining. All three cell type-specific markers, *MAP2, ALCAM* and VE-Cadherin, were expressed in the co-cultures as expected (Fig. 4b). We quantified the populations by flow cytometry and observed similar outcomes, with approximately equal proportions of each cell type (Fig. 4c). These data suggest that cell

types can be differentiated in parallel, in the same media and without additional soluble factors.

Next, we combined the three cell types, inducible *ATOH1, NKX3-1* and *ETV2* hiPSCs, in one culture and induced differentiation. The resulting cells expressed markers for fibroblasts, neurons and vascular endothelial cells (Fig. 4b,c). The proportions of each cell type by flow cytometry were 15.9±0.6% *NCAM*$^+$, 22.6±1.1% *VIM*$^+$ and 38.1±1.6% VE-Cadherin$^+$. We also performed scRNA-seq to assess whether the transcriptomic signatures of the three cell lineages were retained. Therefore, a more sensitive scRNA-seq method was desired rather than maximizing the number of cells analyzed. This was achieved using FACS-based single cell isolation and Smart-seq2 library preparation, which detects more molecules per cell compared to microfluidic-based methods35. We observed three distinct populations, with each one correlating to one induced TF (Fig. 4d). In each population, the TF matched its expected cell type-specific expression signature based on unbiased marker selection because some canonical genes showed weak expression and were not readily detected by scRNA-seq (Fig. 4e). We detected strong cell type–specific transcriptomic signatures in the few cells that were captured. To test parallel programming in three-dimensional culture, we performed similar mixing experiments and generated spheroids. All three lineages appeared, as assessed by microscopy and flow cytometry (Supplementary Fig. 6a,b).

SOX9 programs hiPSCs into induced oligodendrocytes

Organoid technology is limited by the long timelines required for the emergence of certain cell types. In cerebral organoids, for instance, it takes 103 to 210 days for mature myelin to form[36, 37]. There are no reported protocols to differentiate hiPSCs to myelin-producing oligodendrocytes in lineage-independent media using TFs to our knowledge[38, 39]. To address this need with the Human TFome library, we identified 15 TFs involved in oligodendrocyte differentiation and maturation *in vivo* using prior knowledge from developmental biology (Supplementary Table 6). We queried their rank in our screen, which yielded *SOX9* as the top hit. SOX family members have broad roles in the development of various tissues[40, 41] and SOX9 has been used in combination with *NFIB* and soluble factors to induce astrocyte differentiation[42]. However, SOX9 has not been reported, individually or in a combination, to program hPSCs into oligodendrocytes.

At day 4 after *SOX9* induction, hiPSCs were converted to oligodendrocyte progenitors without additional lineage-specifying cues (Fig. 5a). The cells expressed the hallmark oligodendrocyte progenitor marker O4 (82±6%) and were positive for NG2, a glial progenitor marker, by immunostaining (Fig. 5b). Their transcriptomic signatures were similar to primary oligodendrocytes based on unbiased PCA (Fig. 5c), up-regulation of key oligodendrocyte genes (Fig. 5d, Supplementary Table 5) and transcriptomic comparison of highly variable genes (Supplementary Fig. 7a). We also detected expression of the oligodendrocyte lineage markers *CSPG4* (NG2) and *MYRF* by scRNA-seq (Fig. 5e). Pluripotency genes were down-regulated in both scRNA-seq (Fig. 5e) and bulk RNA-seq (Supplementary Fig. 7b).

To assess the myelination potential of SOX9-induced cells, we applied parallel programming to produce an oligo-neuronal co-culture. We combined inducible SOX9 hiPSCs along with

our previously described, fully characterized hiPSC-derived inducible neurons, which project long axons upon differentiation[20]. We then activated TF expression. At 3 dpi, without additional external culture-specific factors, we observed oligodendrocytes contacting axons and beginning the ensheathment process (Supplementary Fig. 7c). Robust myelin sheaths around axons were visualized by TEM after 30 days of co-culture in photo-micropatterned microchannels[43, 44] (Fig. 5f). We computed G-ratios, a metric for compact myelin, to be 0.56±0.02 (Fig. 5g), which are similar to those of the human brain (0.5 to 0.8)[45]. These results confirmed the *in vitro* myelination functionality of SOX9-induced oligodendrocytes.

To evaluate the *in vivo* engraftability and functionality of *SOX9*-induced oligodendrocytes, we transplanted the cells using established methods[39, 46] into Shiverer mice. This congenitally hypomyelinated mouse model has a knockout in the myelin basic protein (*MBP*) gene. We detected engraftment of *SOX9*-induced cells in immunostained brain sections 10 weeks after transplantation based on the presence of *MBP* (Fig. 5h), which can only be expressed in the donor cells. No *MBP* was observed in the control group. Furthermore, based on TEM of brain cross-sections, we observed compact myelin in mice transplanted with *SOX9*-induced cells, but rarely in the control group (Fig. 5i). The number of myelinated axons in mice transplanted with cells was significantly higher compared to the control group (Fig. 5j, $P < 3.1 \times 10^{-5}$).

Taken together, our results demonstrate that induction of *SOX9* alone was sufficient to program hiPSCs cell-autonomously into induced oligodendrocytes. The molecular profiles of the cells with continuous doxycycline administration were similar to those of primary oligodendrocytes, and the cells could form compact myelin in a coculture and in hypomyelinated mice.

Orthogonal programming accelerates the myelination of cerebral organoids

To accelerate myelination in cerebral organoids and construct more accurate models of human brain tissue, we harnessed the *SOX9*-induced oligodendrocytes to introduce the concept of orthogonal cell programming (Fig. 5k). In this approach, cell-autonomous TF overexpression is used alongside a differentiation method that uses external cues (Supplementary Fig. 7d). To this end, we combined inducible *SOX9* hiPSCs with unmodified hiPSCs and induced cerebral organoid formation[47]. After four days, we added doxycycline to induce *SOX9* expression in the orthogonally programmed group and compared it with the control group where *SOX9* was not induced. At 40 dpi, we observed myelin oligodendrocyte glycoprotein (*MOG*) in immunostained cross-sections of orthogonally programmed organoids (Fig. 5l), but not in the controls. TEM on these cross-sections showed robust compact myelin formation in orthogonally programmed organoids (Fig. 5m), confirming that incorporation of *SOX9*-induced oligodendrocytes accelerated myelin maturation. The G-ratio of the myelinated axons was computed to be 0.52±0.04 (Fig. 5n), similar to that of healthy human brains[45].

Discussion

The Human TFome enables systematic investigation of TF-based programming for cell engineering. We conducted a cell type–agnostic screen of the complete library in three hiPSC lines using down-regulation of the pluripotency marker TRA-1-60 as a readout. The screen revealed a more widespread ability of individual TFs to induce differentiation than anticipated, with 290 hits in at least two lines and 65 in all three lines. Our PubMed search indicated that only 49 of the 290 hits have been previously associated with lineage programming, and thus 241 hits have not been reported previously. The cell conversions were rapid (4 days), efficient and induced by single TFs in mTeSR1 medium, without any alteration of soluble factors or mechanical cues.

Among the hits, we discovered four that differentiated hiPSCs into induced neurons, fibroblasts, oligodendrocytes, and vascular endothelial-like cells. To our knowledge, other than work from our laboratories, current protocols for these cell types[25, 38, 39, 48–51] require cell type–specific media components for the initiation of differentiation, even if TFs are also used. The *ATOH1*-induced neurons are similar to those described in our previous work, which were generated using TFs of the *Neurogenin* family[20], in that they do not require neuronal-induction culturing conditions, which is a major advantage. Our *NKX3-1*-induced fibroblast protocol represents an advance in that no TF-based differentiation protocol for fibroblasts has been reported, and current differentiation methods require embryoid body formation, collagen embedding and replating over three weeks of culture with unknown conversion efficiency[48]. Our *ETV2* isoform 2 protocol for vascular endothelial–like cells generates 95% VE-Cadherin^{+} cells compared with ~40% in previous work[49–51], emphasizing the importance of isoforms in cell programming. Our *SOX9*-induced oligodendrocyte protocol is more streamlined and facile compared to a previous TF-based method[38], which required multi-step cell type–specific media conditions to bring hiPSCs to the neural progenitor stage, followed by glial-specific soluble factors to promote oligodendrocyte differentiation.

We found that PiggyBac transposons, which were optimized for high-throughput individual cell line engineering, significantly improved differentiation efficiency compared to lentiviral gene transfer. We demonstrated that long-term TF induction is not required to differentiate cells into a stable cell fate. *ATOH1*-induced neurons and *NKX3*-1-induced fibroblasts were functional *in vitro* (Fig. 2e,f,k,l), and *ETV2*-induced vascular endothelial-like cells were functional *in vivo* (Fig. 3i-k) without continuous TF induction. The practical benefit is the alleviation of long-term replenishment of TF-induction molecules to achieve differentiation and the possibility of excising PiggyBac transposons from the genomes of engineered cells[52].

A major challenge in tissue engineering is the generation of multiple cell types in one culture, especially supporting cells such as fibroblasts or endothelial cells[53]. We showed that our lineage-independent differentiation approach can help address this issue. Previously, liver bud–like tissues containing multiple lineages were produced through heterogeneous expression of *Gata6* in hiPSCs in the same culture[54]. However, control over cell identities and the ratios of each cell type was not attained owing to the lack of genetic switches to tune

these parameters. Parallel programming using TFs discovered from our screen allowed us to achieve high-resolution control over cell type composition and proportion. This enabled co-differentiation of hiPSCs into induced neurons, fibroblasts and vascular endothelial-like cells without lineage-specific cues. We also used parallel programming of induced oligodendrocytes and neurons to rapidly construct robust *in vitro* myelination models, featuring physiological cell-cell interactions.

Further research is needed to understand how cell types differentiated in parallel compare with homogeneously differentiated cells. Although our four protocols could override pluripotency networks to achieve nearly complete differentiation in four days, the resulting cells were not transcriptomically equivalent to their primary-cell counterparts, despite having the expected functionality. We have also not explored whether our approach can mitigate the effects of different media compositions or the variability in differentiation propensity between hiPSC lines[21, 22]. Another important avenue for future research is to investigate how many specialized cell types can be generated by single or combinatorial TF expression.

As demonstrated here, we envisage that the Human TFome will be used in conjunction with other approaches for cell and tissue engineering. As with other genome-scale methods, interpreting the results of Human TFome screens requires information from developmental biology, computational systems biology, cell atlases, functional assays, or other sources. In this study, we referred to the developmental biology literature to understand the specific markers for the four analyzed cell types, to learn that the top hit from our screen, *ATOH1*, is involved in neuronal differentiation, to identify *ETV2* as a driver of vascular endothelial programming, to select 15 TFs involved in oligodendrocyte development, and to validate 49 of our hits as previously associated with differentiation. The systematic, empirical nature of the Human TFome approach is well suited to integration with computational approaches, such as CellNet[9], to iteratively refine cell programming. We used CellNet here to identify the phenotype of our second most efficient hit, *NKX3-1*.

For organoid engineering, our orthogonal programming strategy complements existing methods such as assembloids[55–57], genetic approaches[51, 58] and *in vivo* approaches[59]. We overcame the slow emergence of oligodendrocytes in cerebral organoids by including *SOX9*-induced hiPSCs at the beginning of organoid production. Current protocols for myelinated organoids rely on external developmental signaling and require 103 to 210 days for myelin formation[36, 37]. Orthogonal programming reduced the timeline by more than half, to 40 dpi, to achieve accelerated myelination with mature myelin markers and compact myelin formation with the correct cytoarchitecture. Orthogonal programming may also allow for the incorporation of missing cell types from diverse lineages, distribution of cells more homogeneously within the tissue and fine control over cell proportions, which would all facilitate the adoption of more physiological tissue architecture.

The Human TFome is synergistic with mammalian cell atlases[35, 60–63]. Whereas cell atlas projects ‘read’ cell types and states, the Human TFome enables TF screening aimed at ‘writing’ the cellular programs, and has the potential to produce cell types and states that are currently inaccessible. The concepts presented here enable cross-pollination of tissue

engineering and genomics to discover recipes for each cell type and state throughout development and aging.

Online Methods

Annotation of human transcription factors

A starting set of 1,591 TFs[14] was used, based on their evidence codes “a and b” (confirmed experimental evidence), “c” (prediction only), and “other” (probable TFs with undefined DNA- binding domains). Additional TFs curated by the Human Genome Organization (HUGO) Gene Nomenclature Committee (HGNC)[64] were added: zinc fingers (including those containing C2H2 domains), homeodomains (including LIM, POU, TALE, HOXL, NKL, PRD sub-families), and basic helix-loop-helix and forkhead TFs. Pseudogenes, as annotated by HGNC or Ensembl, were removed. All genes were converted to approved gene names using the HGNC multi-symbol checker. The final set of TFs included in the Human TFome contained 1,564 genes (Supplementary Table 1).

Construction of the Human TFome expression library

Gateway-compatible ORFs for the target set of 1,564 genes were requested from the Vidal lab ORFeome collection[18], the Taipale lab[15], DNASU[16], and transOMIC.com. For the missing ORFs, Uniprot protein sequences of 273 genes were reverse-translated and codon-optimized for synthesis by Gen9 Inc. (Boston, USA). Where multiple isoforms exist, the one designated as “canonical” by Uniprot was selected. If the isoform was longer than 4kb, the longest isoform below 4kb was chosen due to synthesis constraints. Synthesized genes were cloned into pDONR221 using BP Clonase II (Invitrogen, 11789020). All pDONR plasmids are available on Addgene, DNASU or transOMIC. TF Sources are summarized in Supplementary Fig. 1a. To determine the tissue expression of synthesized TFs, GTEx[65] version 6 median tissue FPKMs were downloaded. For each TF, its median expression across tissues was computed. TFs that were synthesized were compared to TFs that were cloned from cDNAs.

Pooled library cloning into lentiviral expression vector

All pDONR-TFs were pooled and cloned into pLIX_403, the doxycycline-inducible lentiviral vector (a gift from David Root, Addgene plasmid # 41395), using LR Clonase II (Invitrogen, 11789100), transformed into Stbl3 chemically-competent cells (Invitrogen, C737303), and spread on LB agar plates containing 100μg/μl carbenicillin (Teknova, E0096). Colonies were counted to ensure library coverage of >200×, scraped, resuspended in PBS, and plasmids were extracted using the endotoxin-free Midi Prep plus kit (QIAGEN, 12943). DNA was quantified using the Qubit dsDNA broad range kit (Invitrogen, Q32853). To determine coverage, pDONR-TF and pLIX_403-TF pools were prepared for next-generation sequencing using NEBNext Ultra DNA Library Prep Kit for Illumina (New England Biolabs, E7370L). Libraries were quantified using the KAPA Real-Time Library Amplification kit (Roche, KK2702) and loaded onto an Illumina MiSeq v3 150-cycle kit (MS-102-3001). About 97% of the TFs fit within the pLIX_403 vector cargo limit of approximately 4kb (Supplementary Fig. 1e). The TF library was subcloned into the lentiviral expression vector with even representation and high coverage (Supplementary Fig. 1f-h).

Data processing and analysis for library cloning

To align reads to the TFome library, reference TF sequences were first indexed using the STAR aligner v2.5.2a7 using the command STAR --runMode genomeGenerate with parameter -- genomeSAindexNbases 9 to accommodate a reference “genome” with fewer bases, as recommended in the manual. Reads were aligned to the reference index using the STAR command, counted using bash scripts, and plotted in R.

Cell culture

The PGP1 hiPSC line without integrated Yamanaka factors was generated from adult dermal fibroblasts from a 55 year old male (Coriell, GM23248)[66] and the CRTD5 hiPSC line[67] was generated from foreskin fibroblasts (ATCC CRL-2522), both using the CytoTune 2.0 Sendai Reprogramming Kit (Invitrogen, A16517). Cells were adapted to feeder-free culture, verified for pluripotency by flow cytometry, and karyotyped. The ATCC DYS0100 hiPSC (ACS-1019 DYS0100) hiPSC was obtained from ATCC. Cell lines were verified by short tandem repeat (STR) profiling (Dana Farber Cancer Institute), regularly verified to be mycoplasma-free using the Universal Mycoplasma Detection Kit (ATCC, 30-1012K), and cultured between passages 8 and 40. hiPSCs were cultured in mTeSR1 (STEMCELL Technologies, 05850) without antibiotics on tissue-culture-treated plates coated with Matrigel (Corning, 354277) and media was changed daily. hiPSCs were passaged using TrypLE Express (Life Technologies, 12604013), and seeded with Y-27632 ROCK inhibitor (Millipore, 688001) for one day. Cells were frozen using mFreSR (STEMCELL Technologies, 5854) using a CoolCell LX (Biocision, BCS-405) overnight at −80°C, then in vapor-phase liquid nitrogen for long-term storage. PBAN, a Gateway-compatible, doxycycline-inducible, puromycin-selectable PiggyBac vector was constructed from PB-TRE-dCas9-VPR (Addgene #63800) and used to deliver TFs to hiPSCs using a Lonza Nucleofector X-Unit (AAF-1002X) following the manufacturer’s instructions. Electroporated cells were transferred to a 6-well Matrigel-coated plate in mTeSR1 with ROCK inhibitor. Cells were selected with 1μg/ml puromycin (Gibco, A1113803).

Flow cytometry and fluorescence-activated cell sorting (FACS)

For flow cytometry analysis and FACS, cells were dissociated using TrypLE Express, washed, and resuspended in FACS buffer (PBS with 10% FBS). For surface antigens, live cells were stained with fluorophore-conjugated antibodies and CellTrace Calcein Blue, AM (Life Technologies, C34853) at 1×10^7 cells/ml for 30 minutes on ice in the dark. For intracellular staining, cells were fixed using BD Cytofix fixation buffer (BD Biosciences, 554655) at 1×10^7 cells/ml for 20 minutes, washed with BD Perm/Wash buffer (BD Biosciences, 554723), and permeabilized in BD Perm/Wash buffer for 10 minutes, then stained with fluorophore-conjugated antibodies and DAPI in the dark for 30 minutes. Stained cells were washed twice with FACS buffer, filtered into a strainer-capped tube (Falcon, 352235), and run on a BD LSRFortessa. FACS was performed on a BD FACSAria or Beckman Coulter MoFlo Astrios. Spectral overlap was compensated using single fluorophore-conjugated AbC Total Antibody Compensation Beads (Life Technologies, A10497) with single fluorophore-conjugated antibodies. All antibodies are listed in Supplementary Table 6. Flow cytometry data was analyzed using FlowJo 10.2.

Lentiviral production and transduction

Lentiviral particles were produced as previously described68 as one pool containing the complete Human TFome library. Particles were produced by transfecting polyethylenimine (PEI; Polyscience, 24765), pMD2G (Addgene plasmid 12259), psPAX2 (Addgene plasmid 12260), and pLIX_403-TFs into 293T cells. Media was exchanged after 24h and supernatants were harvested at 48h and 72h post-transfection. The supernatants were filtered (0.45-mM PES filter, Corning 431220) and combined. Viral particles were then precipitated at 4°C overnight using PEG solution (BioCat, K904-50-BV). The lentiviral particles were resuspended with PBS in 1/100 of the supernatant volume (100× concentrated). Alternatively, lentiviral particles were concentrated by ultracentrifugation as previously described[68]. The particles were transferred as 50 µl aliquots into 1.5-ml screw-cap tubes, snap-frozen on dry ice and stored at −80°C. Titrations were performed by qPCR as previously described[68]. The titers ranged between 1×10^6 and 6×10^7 IFU/ml. To transduce the entire library to achieve single copy integrations, we used a large hiPSC population so that on average every TF was theoretically represented by >100 cells. 750,000 PGP1, ATCC-DYS0100 and CRTD5 hiPSCs were each transduced with 75,000 lentiviral particles (multiplicity of infection (MOI) = 0.1) in mTeSR1 media (two 6-well plates per pool). The low MOI ensures that most cells are not transduced (and are hence selected against by puromycin) and the cells that are transduced are most likely to receive only a single TF. Culture medium was exchanged daily. 48h post transduction, 3 µg/ml of puromycin was added to the media to eliminate non-transduced PGP1 cells. Cells were maintained and propagated as mentioned before.

TFome screen using FACS

Each independently transduced hiPSC population was expanded into three 10-cm dishes, representing 3 replicates (Supplementary Fig. 2a). Each dish was seeded with 2 million cells in mTeSR1 with ROCK inhibitor, 0.5µg/ml doxycycline, and 1µg/ml puromycin. The next day and daily thereafter until 4 dpi, the media was replenished with mTeSR1 containing doxycycline. As hiPSCs became confluent at 4 dpi, this day was chosen for dissociation and staining. Cells were not passaged for longer culture because of the faster proliferation rate of hiPSCs, which may out-compete differentiated cells. Cells were then dissociated using TrypLE Express, and counted using an automated cell counter (ThermoFisher Scientific, Countess II, AMQAX1000). Typically, 10 million live cells were harvested per 10cm dish, stained for PE anti-TRA-1-60 and Calcein AM (Life Technologies, C1430) in mTeSR1 media at 10^7 cells/ml for 30 minutes in the dark, washed, and then filtered for debris using a single-cell strainer (Falcon, 352253). Cells were sorted on a BD FACSAria or Beckman Coulter MoFlo Astrios. After gating Calcein AM-positive cells, cells in the bottom 10% and the middle 50% of TRA-1-60 expression were designated as TRA-1-60^{low} (differentiation gate) and TRA-1-60^{high} (stem cell gate), respectively. Approximately 0.8 million TRA-1-60^{low} and 4 million TRA-1-60^{high} cells were collected for each replicate in the whole-library screen. Cells were subsequently spun down and the cell pellet was frozen at −20°C.

Genomic extraction, PCR and library preparation for sequencing

Genomic DNA was extracted from sorted cells using the DNeasy Blood & Tissue Kit (Qiagen, 69506) on a QIAcube (Qiagen). >5 μg of genomic DNA was used for PCR and subsequently purified using the QIAquick PCR purification kit (Qiagen, 28106) on a QIAcube. Purified DNA was quantified using the Qubit dsDNA broad range quantification kit (ThermoFisher Scientific, Q32853). 1 μg of DNA was sheared to an average of 200bp on a Covaris sonicator E220 and used for library preparation using NEBNext Ultra DNA Library Prep (New England Biolabs, E7370). Samples were sequenced on an Illumina NextSeq 500 on high-output mode (Supplementary Table 2) with high coverage (Supplementary Fig. 1j).

Analysis of sequencing data from TFome screening

Sequencing reads of amplified TFs were aligned to reference sequences using STAR aligner v2.5.2a[69]. The ratio of cells in TRA-1-60 high versus low gates was used as an indicator of loss of pluripotency above basal spontaneous differentiation for each TF, as the TRA-1-60 high fraction served as an internal control. A $\log_2(\text{TRA-1-60}^{low}/\text{TRA-1-60}^{high})$ score was computed using DESeq2[70]. A statistical threshold for defining TFs as hits was determined based on maximizing enrichment compared to random sampling as follows: for each cell line, TFs were ordered by their $\log_2(\text{TRA-1-60}^{low}/\text{TRA-1-60}^{high})$ score. Then, an enrichment score was computed for each candidate threshold. The enrichment score is computed by the number of TFs above that threshold in at least two cell lines minus the number of TFs above that threshold in a randomized dataset (n = 10,000 random samples). The enrichment scores for a set of candidate thresholds is plotted in Supplementary Figure 2d. A threshold of 25% had the highest enrichment score.

Literature search to determine novelty of hits

To determine if a TF hit was novel for its ability to induce differentiation or forward programming upon overexpression, the name of each TF hit and the terms “differentiation”, “programming” or “overexpression” were queried in PubMed on April 26, 2020. TFs were considered “known” if at least one paper reported that the overexpression of the TF alone, or in combination with other factors, promoted the differentiation of one cell type into another; otherwise, the TF was considered novel. TFs having knockout studies alone without overexpression evidence were considered novel.

Immunofluorescence microscopy

Cells were immunostained as previously described[20]. Cells were grown on Matrigel-coated 12 mm coverslips (Warner Instruments, CS-12R15), fixed with 4% PFA (Electron Microscopy Sciences, 15714-S) in PBS for 20 minutes at room temperature, washed three times with PBS, and kept at 4°C submerged in PBS until staining. Fixed samples were incubated with a blocking solution containing 10% normal donkey serum (Millipore, S30-100ml), 1% BSA, and 0.5% Triton X-100 in 1× PBS for 1 hour at room temperature, or overnight at 4°C. The stain buffer was similar to the block solution, except the concentration of normal donkey serum was reduced to 3%. Coverslips were incubated at room temperature for 1 hour with the stain buffer containing primary antibodies, then washed with stain buffer

twice, incubated with secondary antibodies in stain buffer at room temperature for 1 hour, and washed once with stain buffer and twice with PBS. Coverslips were mounted on glass slides by incubating with Prolong Diamond Antifade with DAPI (Invitrogen, P36966), incubated overnight at room temperature in the dark, and sealed with nail polish (Electron Microscopy Sciences, 72180). Mounted coverslips were imaged on a Zeiss Observer.Z1 microscope equipped with a LD Plan-Neofluar 40×/0.6 objective, a four-channel LED light source (Colibri), and an EM-CCD digital camera system (Hamamatsu). Antibodies are listed in Supplementary Table 6.

Bulk RNA sequencing library preparation

600 μl TRIzol (Life Technologies, 15596-018) was added directly to cells, which were then incubated for 3 minutes and used for RNA extraction using Direct-zol RNA MiniPrep following the manufacturer's recommendations (Zymo Research, R2050). RNA was quantified using the Qubit RNA HS Kit (Molecular Probes, Q32852), and RNA integrity was confirmed by the presence of intact 18S and 28S bands on a 1% E-Gel EX (Invitrogen, G402001). 1 μg RNA was used for Poly(A) isolation using the NEBNext Poly(A) mRNA Magnetic Isolation Module (New England Biolabs, E7490L) and the NEBNext Ultra Directional RNA Library Prep Kit for Illumina (New England Biolabs, E7420L). Library size was visualized on a 1% E-Gel EX, and quantified using the KAPA Library Quantification Kit as described before. Samples were sequenced on an Illumina NextSeq500 on High-Output mode.

Analysis of Bulk RNA sequencing data

A STAR human transcriptome reference index was generated using Gencode GRCh38.primary (ftp://ftp.sanger.ac.uk/pub/gencode/Gencode_human/release_25/GRCh38.primary_assembly.genome.fa.gz) as the genome sequence and Gencode v25 transcript annotations (ftp://ftp.sanger.ac.uk/pub/gencode/Gencode_human/release_25/gencode.v25.annotation.gtf.gz). RNA-seq reads were aligned on four 12 Gb cores using the command: STAR -quantMode GeneCounts. Gene counts per sample were merged into a master table and analyzed in R version 3.2.2. Differential expression analysis was performed using DESeq2[70]. Log_2 fold changes and standard errors were estimated using DESeq2. The default Wald's test was used for statistical testing, independent filtering and p-value adjustments. Heatmaps were generated in R using the gplots and RColorBrewer packages. Default settings were used for scaling, coloring and clustering. CellNet[9] was used on FASTQ files to classify cell types using default settings. FASTQ files are available on NCBI GEO (see Data Availability).

Comparison of RNA data to reference datasets

Bulk RNA-seq raw data for *ATOH1, NKX3-1, ETV2* and *SOX9*-induced cells and external reference datasets were processed consistently using the identical pipeline for gene expression quantification. Gene expression profiles of *ATOH1*-induced neurons were compared to human brain samples from the ENCODE Project (ENCSR239GFM for hippocampus, ENCSR274JRR for brain). *SOX9*-induced oligodendrocytes were compared to newly formed oligodendrocytes (NFO), myelinating oligodendrocytes (MO) and oligodendrocyte precursor cells collected from mouse brain[71] (GSE52564). *NKX3-1*-

induced fibroblasts were compared to fibroblasts[21] (GSE73211). ETV2-induced endothelial cells were compared to HUVECs[72] (GSE93511). Gene counts were calculated by RSEM (1.3.3)[73] using the --star option allowing to align reads with STAR (2.7.3a) on the GRCh38 reference genome and Ensemble annotation 94. Secondary analyses were performed in the statistical R environment (v3.6.1). TPM value from RSEM output was used for gene filtering and PCA analysis. Genes with more than 10 counts per million in at least 3 samples were retained. For the comparison between *SOX9*-induced cells and mouse OPCs, only homologous genes between the two species annotated in the Mouse Genome Database[74] (http://www.informatics.jax.org/downloads/reports/HOM_MouseHumanSequence.rpt) were retained. A DESeq2[70] object was created providing the cell line information in the design formula. PCA was then performed on vst transformed[75] and SVA batch corrected[76] TPM values using the prcomp function. Removal of hPSCs prior to PCA analysis did not affect the separation between differentiated and primary cells.

Electrophysiology

Assessment of neuronal function was performed as previously described[20] with minor modifications. Rat astrocytes (Gibco, N7745100) were seeded onto Matrigel-coated coverslips and cultured in DMEM with GlutaMAX, 10% FBS, and N2 supplement (Gibco, 17502048). One day before seeding induced neurons, astrocytes were cultured in Neurobasal media with GlutaMax and B27 supplement (Gibco, 17504044). *ATOH1* hiPSCs were labeled by lentiviral transduction of constitutively expressed GFP (FUGW, Addgene 14883). 500,000 GFP-labelled *ATOH1* hiPSCs were seeded in a 6-well tissue culture plate and induced with doxycycline for three days on Matrigel-coated coverslips, then dissociated using TrypLE Express. Cells were counted and 1 million induced neurons were plated in pre-conditioned media on astrocytes. Media was changed twice weekly. Electrophysiological recordings were carried out at 20–25°C on an upright Olympus BX51WI microscope. Cells were bathed in artificial cerebrospinal fluid (ACSF) containing (in mM) 119 NaCl, 2.5 KCl, 4 $CaCl_2$, 4 $MgSO_4$, 1 NaH_2PO_4, 26.2 $NaHCO_3$, and 11 glucose, saturated with 95% O_2/5% CO_2. Intracellular recordings were obtained using 3- to 5-MΩ glass micropipettes filled with an internal solution containing (in mM) 136 $KMeSO_3$, 17.8 HEPES, 0.6 $MgCl_2$, 1 EGTA, 4 Mg-ATP, and 0.3 Na-GTP. Traces were collected using a MultiClamp 700B amplifier (Molecular Devices), filtered with a 2 kHz Bessel filter, digitized at 10 kHz using a Digidata 1440A digitizer (Molecular Devices), stored using Clampex 10 (Molecular Devices), and analyzed off-line using customized procedures in Igor Pro (WaveMetrics). Cells were assessed for the presence of spontaneous action potentials in current-clamp mode. In the absence of spontaneous action potentials, cells were assessed by the injection of a set of 0.6 s current steps, ranging from −140 pA to 400 pA in 60 pA increments.

Wound healing scratch assay

Wound healing scratch assays were performed as previously described[30]. *NKX3-1* cells grown for four days in mTeSR1 either with or without doxycycline were scratched using a P200 tip. Scratches were imaged by a Nikon Eclipse TE200 using a Nikon Plan Fluor 4x/0.13 objective with a Zeiss AxioCam ICm1 camera on days 0, 1 and 2 after scratching. Scratch areas were quantified in an unbiased and automated manner in Fiji[77] using the

Wound Healing plugin (http://dev.mri.cnrs.fr/attachments/download/1992/MRI_Wound_Healing_Tool.ijm). Five scratches were made per well, and the wound areas were averaged to generate one data point per well.

Collagen contraction assay

Collagen contraction assays were performed as previously described[78]. Briefly, NKX3-1 cells grown for four days in mTeSR1 either with or without doxycycline were dissociated and counted. 400,000 cells in 300 µl mTeSR1 were mixed with 150 µl collagen type I diluted to 3 mg/ml (BD, 354236) and 2 µl 1M NaOH, and seeded into a 24-well plate used as a mold. Collagen gels were allowed to solidify at room temperature for 20 minutes. Subsequently, 500 µl mTeSR1 was slowly added. Gels were dissociated from the mold by running a P200 tip along the edge of the well. The plate was then incubated overnight. Thereafter, images were captured using a Zeiss Axio Zoom.V16 Stereo Zoom Microscope with a color AxioCam MRm camera and a PlanNeoFluar Z 1×/0.25 objective. The area covered by the gel was quantified in Fiji[77].

Isoform analysis

For isoform identification, the Gencode v25 basic annotations were used. “Transcript” annotations with the “protein_coding” tag were selected. Only those with a transcript support level of 1 were retained. Annotations with identical consensus coding DNA sequences (CCDS) were collapsed into one isoform. To quantify *ETV2* genomic copy numbers, digital droplet PCR was performed using the Biorad QX100. 15 ng of genomic DNA was used per reaction with ddPCR supermix (Biorad, 1863026), primers to amplify and HEX probe against RPP30 (Biorad, 10031243), primers and FAM probe against puromycin (forward primer: 5’- TGCAAGAACTCTTCCTCACG, reverse primer: 5’- CGATCTCGGCGAACACC, FAM probe: 5’ ACATCGGCAAGGTGTGGGTCG), and AluI (New England Biolabs, R0137S).

Single cell RNA sequencing library preparation

Single cell RNA sequencing of *ETV2* and *SOX9* cells was performed using the Chromium Single Cell 3’ Library & Gel Bead Kit v2 (10x Genomics, PN-120237). ETV2 cells were grown for four days in mTeSR1 with or without doxycycline, dissociated with TrypLE Express, passed through a 35µm cell strainer (Falcon, 352235) and counted. Approximately 1,500 cells, which consisted of an equal mixture of induced and non-induced *ETV2* hiPSCs as well as a spike-in control population of *NKX3-2*-expressing cells, were loaded onto a Chromium chip. *SOX9* cells were grown for four days in mTeSR1 with or without doxycycline, dissociated, passed through a 35µm cell strainer and counted. Approximately 3,000 cells were loaded onto a Chromium chip. Libraries were prepared according to the manufacturer’s instructions, and sequenced on an Illumina NextSeq500 on High-Output Mode.

Single cell RNA-seq of parallel programmed cultures containing *ATOH1, ETV2* and *NKX3-1* cells were processed following the Smart-seq2 workflow as described previously[79]. Briefly, single cells were FAC-sorted into a 96-well plate containing 2 µl of nuclease free water with 0.2% Triton-X 100 and 4 U murine RNase Inhibitor (NEB), spun down and

frozen at -80°C. After thawing, 2 µl of a primer mix was added (5 mM dNTP (Invitrogen), 0.5 uM dT-primer [C6-aminolinker-AAGCAGTGGTATCAACGCAGAGTCGAC TTTTTTTTTTTTTTTTTTTTTTTTTTTTTTVN, where N represents a random base and V is any base besides thymidine], 4 U RNase Inhibitor (NEB)). Next, the RNA was denatured for 3 minutes at 72°C and wells were filled up to 10 µL with RT buffer mix for a final concentration of 1x Superscript II buffer (Invitrogen), 1 M betaine, 5 mM DTT, 6 mM $MgCl_2$, 1 µM TSO-primer (AAGCAGTGGTATCAACGCAGAGTACATrGrGrG, where rG stands for ribo-guanosine), 9 U RNase Inhibitor and 90 U Superscript II. After reverse transcription performed at 42°C for 90 minutes, the reverse transcriptase was heat inactivated at 70°C for 15 minutes and the cDNA was amplified using the KAPA HiFi HotStart Readymix (Peqlab) at a final 1x concentration using 0.1 µM UP-primer (AAGCAGTGGTATCAACGCAGAGT). Cycling conditions were: initial denaturation at 98°C for 3 min, 23 cycles (98°C 20 sec, 67°C 15 sec, 72°C 6 min) and final elongation at 72°C for 5 min. Amplified cDNA was purified using a 1x volume of Sera-Mag SpeedBeads (GE Healthcare) resuspended in a buffer consisting of 10 mM Tris, 20 mM EDTA, 18.5 % (w/v) PEG 8000 and 2 M sodium chloride solution and eluted in 12 µl nuclease-free water. cDNA concentration after purification was measured using a Tecan plate reader Infinite M $Nano^+$ plate reader in black flat-bottom low-volume 384-well plates (Corning) using AccuBlue Broad range chemistry (Biotium). For library preparation, up to 700 pg of cDNA was desiccated and rehydrated in 1 µl Tagmentation mix (1x TruePrep Tagment Buffer L, 0.1 µl TruePrep Tagment Enzyme V50; from TruePrep DNA Library Prep Kit V2 for Illumina; Vazyme) and tagmented at 55°C for 5 min. Subsequently, Illumina indices were added during PCR (72°C 3 min, 98°C 30 sec, 13 cycles [98°C 10 sec, 63°C 20 sec, 72°C 1 min], 72°C 5 min) with 1x concentrated KAPA Hifi HotStart Ready Mix and 300 nM dual indexing primers. After PCR, libraries were quantified with AccuBlue Broad range chemistry, equimolarly pooled and purified twice with 1x volume Sera-Mag SpeedBeads, followed by Illumina sequencing on a NextSeq500 aiming at an average sequencing depth of 400,000 reads per cell. Library preparation was successful for 95 cells and the sequencing yielded an average of 399,000 reads per cell.

Analysis of single cell RNA sequencing data

Analysis of single cell expression matrices was performed on Python notebooks using custom functions and the package Scanpy v1.4.3[80]. Raw matrices were processed with filtering steps to obtain cells with high quality reads (see below). Expression values were then normalized to 10^6 (except for Smart-seq2 data) and log-transformed. Highly variable genes were then selected for downstream visualization and clustering analysis. Biological cell-to-cell variation was linearly regressed out based on counts per cell and percentage of mitochondrial genes and count values were scaled to a maximum value of 10. After dimensionality reduction, processed matrices were used for cluster analysis and visualization. Marker genes were computed by Student's t-test between each cluster and all the other cells.

For *ETV2* and *SOX9* datasets, the 10x Chromium pipeline was used. Reads were mapped to the human genome (GRCh38) and count matrices were generated using CellRanger v2.0.0. For the *ETV2* dataset, low-quality cells were filtered out if they had <200 genes expressed,

<50000 read counts or >0.1% of reads mapped to mitochondrial genes. Clusters were computed by the Leiden algorithm (resolution=0.1) on the neighbor graph computed on the first 10 principal components. Spike-in control *NKX3-2* cells were removed based on clustering for further analysis and visualization. For the *SOX9* dataset, the two matrices arising from different sequencing runs were concatenated. Low-quality cells were filtered out if they had <1200 or >5000 genes expressed, <20000 read counts or <0.08% of reads mapped to mitochondrial genes. Clusters were computed by the Leiden algorithm (resolution=0.2) on the neighbor graph computed on the first 10 principal components.

For the parallel programming dataset of *ATOH1, ETV2* and *NKX3*-1 cells co-cultured in 2D, the data was analyzed using a pipeline developed in house. Briefly, reads were quality-checked by FastQC (https://www.bioinformatics.babraham.ac.uk/projects/fastqc/) and mapped using STAR v2.5.4a to the Ensembl GRC38v94 human genome reference sequence[69]. The Picard v2.9.0 tool CollectRnaSeqMetrics was used to inspect the abundance of ribosomal RNA in each cell (http://broadinstitute.github.io/picard/). The raw expression matrix of cells by genes was then computed using featureCount81 for genes annotated on the Ensembl GRC38v94 genome (ftp://ftp.ensembl.org/pub/release-94/gtf/homo_sapiens/Homo_sapiens.GRCh38.94.gtf.gz). Low-quality cells were filtered out if they had <2000 genes expressed, <50000 counts or >0.3% of reads mapped to mitochondrial genes. Cell clusters were computed with the Leiden algorithm (resolution=0.2) on the neighbor graph computed on the first 7 principal components.

Angiogenesis assay and transmission electron microscopy

For endothelial angiogenesis assays, *ETV2* isoform 2 hiPSCs were induced for 4 days. Then, 70,000 cells were seeded into 48-well plates containing coverslips coated with 100 µL Matrigel and cultured overnight in EGM-2 BulletKit (Lonza, CC-3162) with 0.5µg/ml doxycycline to induce tube formation. For epifluorescence imaging, cells were incubated with Calcein Blue AM (ThermoFisher, C34853), fixed in 4% PFA, washed with PBS, and imaged. For transmission electron microscopy, cells were fixed overnight in 2.5% Glutaraldehyde, 1.25% Paraformaldehyde and 0.03% picric acid in 0.1M sodium cacodylate buffer (pH 7.4) at 4°C. Cells were then washed in 0.1M cacodylate buffer and post-fixed with 1% osmium tetroxide (OsO4)/1.5% potassium ferrocyanide (KFeCN6) for 1?hour. They were subsequently washed twice in water and once in maleate buffer, incubated in 1% uranyl acetate in maleate buffer for 1 hour, washed twice in water, dehydrated in the following grades of alcohol (10 minutes each: 50%, 70%, 90% and twice in 100%). Samples were then placed in propyleneoxide for 1 hour, and infiltrated overnight in a 1:1 mixture of propyleneoxide and TAAB Epon (Marivac Canada Inc. St Laurent, Canada). The following day, samples were embedded in TAAB Epon and polymerized at 60°C for 48?hours. Ultrathin sections (~80 nm) were cut on a Reichert Ultracut-S microtome, picked up onto copper grids stained with lead citrate and examined using a JEOL 1200EX transmission electron microscope. Images were recorded with an AMT 2k CCD camera.

In vivo vascular network-forming assay

Six-week-old nude mice were purchased from Jackson Laboratories (Boston, MA) and housed in compliance with Boston Children's Hospital guidelines. All animal-related

protocols were approved by the Institutional Animal Care and Use Committee. *ETV2* cells for implantation were expanded for 7 days *in vitro* after differentiation and mixed with human mesenchymal stromal cells at a 1:1 ratio for a total of $2x10^6$ cells per mouse in 200 µl of pH-neutral pre-gel solution containing 3 mg/mL bovine collagen I (Trevigen, Cat No. 3442-050-01), 3 mg/mL fibrinogen (Sigma, Cat No. F8630), and 50 µl Matrigel (Corning, Cat No. 354234)[82, 83]. During anesthesia, mice were subcutaneously injected first with 50 µl of 10 U/mL thrombin (Sigma, Cat No. T4648) and then with 200 µl cell-laden pre-gel solution into the same site. All experiments were carried out in 5 mice and explants were harvested after 1 week. Human mesenchymal stromal cells were isolated from the white adipose tissue and cultured on uncoated plates using MSCGM (Lonza, Cat No. PT-3001) supplemented with 10% Gencode FBS (Genesee, Cat No. 25-514), and 1x penicillin-streptomycin-glutamine (PSG, ThermoFisher, Cat No. 10378106). All experiments were carried out using passage 6-10 h-MSCs.

Explanted grafts were fixed overnight in 10% buffered formalin, embedded in paraffin, and sectioned at a thickness of 7 µm. Microvessel density (vessels/mm^2) was defined as the average number of erythrocyte-filled vessels in H&E-stained sections collected from the middle of the implants as previously described[82, 83]. For immunostainings, sections were deparaffinized and antigen retrieval was carried out for 30 minutes with boiling citric buffer (10 mM sodium citrate, 0.05% Tween 20, pH 6.0). Sections were then blocked for 30 minutes in 5% horse serum and incubated with primary antibodies for 30 minutes at room temperature. Fluorescent staining was performed using fluorophore-conjugated secondary antibodies followed by DAPI counterstaining for 30 minutes at room temperature. Human-specific anti-CD31 (Dako, M0823) was used to stain human blood vessels. Perivascular cells were stained by anti-alpha smooth muscle actin antibody (Abcam, ab5694). Images were acquired using an Axio Observer Z1 inverted microscope (Carl Zeiss) and AxioVision Rel. 4.8 software. Fluorescent images were acquired using an ApoTome.2 Optical sectioning system (Carl Zeiss) using a 20x objective lens.

In vitro myelination assay

SOX9-induced oligodendrocytes were co-cultured with iNGN hiPSC-derived neurons[20] to assess myelin formation. To facilitate the preparation of cross-sections of myelinated axons, these cells were co-cultured within a microchannel mold that promotes the alignment of axons along the channel in one direction. The microchannel mold was constructed by adding a 10% (w/v) PEG-diacrylate (Mn 1000; Polysciences Inc., Warrington, PA) and 0.5% (w/v) Irgacure 2959 in PBS solution to a collagen-coated transwell[43, 84, 85]. A negative mask was used to create the microchannel, followed by irradiation of the light-sensitive media with 181 mW/cm2 UV light for 30 seconds. SOX9 and iNGN hiPSCs were then seeded into the microchannel and TFs were induced by doxycycline. The coculture was maintained in mTeSR1 for the first four days and then the media was replaced to preserve long term oligo-neuronal culture with the following components: DMEM-F12 with 1:200 N2 supplement, 1:100 B27 supplement lacking vitamin A, 1% penicillin/streptomycin/glutamine, 60 ng/mL T3, 10 ng/mL NT3, 10 ng/mL IGF-I, 200 µM AA, 1:1000 Trace Elements B, 2 ng/mL BDNF and 2 ng/mL GDNF[39]. After four weeks of co-culture, the constructs were fixed,

embedded in resin, sectioned, stained and imaged using transmission electron microscopy as described above for the angiogenesis assay.

In vivo engraftment and myelination assay

Homozygous Shiverer mice[46] were purchased from Jackson Laboratories (Stock No. 001428), housed under appropriate conditions and were crossed with heterozygous mice adhering to Harvard Medical School guidelines. All animal protocols were approved by the Institutional Animal Care and Use Committee. 4-day doxycycline-induced SOX9 cells were live stained[86] using 1:10 O4 antibody and were sorted for O4-positive cells using Sony SH800s cell sorter. Neonatal mice (postnatal days 1-2) were cryo-anesthesized and 50,000 O4-positive cells resuspended in 2 μL PBS were injected intracranially by freehand injection[46]. Control animals received PBS injections. Pups in both control and experimental groups were confirmed to be homozygous Shiverer both by their phenotype and through genotyping and were euthanized for further analysis after 10 weeks using perfusion with 4% PFA. Tissue sections were obtained and embedded for antibody staining. Briefly, the brain sections were deparaffinized and an antigen retrieval process was done in a sodium citrate buffer at 95°C for 30 minutes. The slides were then blocked with 10% normal goat serum in 1% BSA in PBS for 30 minutes at room temperature, followed by staining using anti-MBP antibodies in 1% BSA in PBS overnight at 4°C. The following day, the slides were washed with PBS and incubated with 1:250 biotinylated goat anti-rat secondary antibodies. After multiple washing steps, the slides were counterstained by hematoxylin, dehydrated and mounted. To perform electron microscopy on the brain tissue, the injection site was used as a landmark to prepare the tissue for sectioning. The rest of the process was done similar to what has been described earlier for electron microscopy.

Parallel cell programming in two-dimensional culture

For immunofluorescence microscopy, *ATOH1, ETV2* and *NKX3-1* hiPSCs were mixed and seeded in all combinations at equal ratios in mTeSR1 and Y-27632 ROCK inhibitor with or without 0.5μg/mL doxycycline on Matrigel-coated 10-mm circular coverslips in 12-well plates. In total, 60,000 cells were seeded in wells for non-induced controls and 180,000 in wells for doxycycline induction. mTeSR1 with or without doxycycline was replenished each day. After 4 days, the medium was removed, and cells were washed with PBS (without magnesium or calcium) at room temperature, and fixed in 4% PFA (Electron Microscopy Sciences, 15714-S) in PBS for 15 minutes at room temperature. Coverslips were blocked with 200 μl 10% Normal Donkey Serum (NDS, Millipore, S30-100ml) in PBS for 20 min, and incubated for 90 minutes at room temperature with the following primary antibodies (Supplementary Table 6) diluted in 3% NDS in PBS: 1:400 rabbit anti-VE-Cadherin, 1:500 chicken anti-MAP2, 1:400 goat anti-ALCAM. After three 10-minute washes with 200 μl PBS, coverslips were incubated for 45 minutes at room temperature with fluorophore-conjugated secondary antibodies (1:500 dilution) and 1 mg/ml DAPI (Roche, 10236276001) in 3% NDS: donkey anti-chicken Cy3, donkey anti-rabbit Alexa Fluor 488, donkey anti-goat Alexa 647. Coverslips were then mounted on microscopy slides using AquaMount (VWR, 41799-008) and stored overnight in the dark at room temperature. Thereafter, slides were imaged with an Axio Observer.Z1 microscope with motorized stage (Carl Zeiss Microscopy, Jena, Germany) using 20× and 40× air objectives. Images were stored in the manufacturer's

format (.czi) and were subsequently exported to the *.jpeg format using the ZEN blue software (Carl Zeiss Microscopy).

For flow cytometry and single cell sorting, *ATOH1, ETV2* isoform 2 and *NKX3-1* hiPSCs were mixed and seeded in all combinations in mTeSR1 and Y-27632 ROCK inhibitor with or without 0.5μg/mL doxycycline on Matrigel-coated 12-well plates. In total, 30,000 cells were seeded in wells for non-induced controls and 90,000 in wells for doxycycline induction. mTeSR1 with or without doxycycline was replenished daily. After 4 days, cells were dissociated with TrypLE Express, re-suspended with 1 ml PBS per well, transferred to strainer-capped tubes for flow cytometry, and spun-down for 4 minutes at 1400 RPM. Next, the supernatant was aspirated, and cells were immunofluorescently labeled with fluorophore-conjugated antibodies (Supplementary Table 6) against NCAM (1:20), Vimentin (1:20) and VE-Cadherin (1:20) diluted in 100 μl 0.2 μm-filtered FACS buffer (1% BSA (Albumin fraction V; Roth, 8076.2), 2 mM EDTA, in sterile PBS pH 7.4) for 1 hour at 4°C in the dark. Cells were spun down for 4 minutes at 1400 RPM, washed with FACS buffer once, spun down again and re-suspended in 250 μl FACS buffer. Tubes were kept on ice until analysis within the following hour on a BD FACSAria II. Additionally, 95 single cells were sorted in a 96-well plate with a BD FACSAria III (100 μm nozzle) and sent for single cell sequencing at the CMCB Deep Sequencing Facility.

Parallel cell programming in embryoid bodies

24-well Aggrewell plates (STEMCELL Tech, 34450) were prepared following the manufacturer's protocol. *ATOH1, ETV2* isoform 2 and *NKX3-1* hiPSCs were seeded in equal ratios in Aggrewell EB Formation Medium (STEMCELL Tech, 05893) with Y-27632 ROCK inhibitor (Millipore, 688001). A total of $6x10^5$ cells was used. 50% Aggrewell EB Formation Medium was changed daily. After 4 days, the EBs were harvested and transferred into ultra-low attachment wells (Sigma, CLS3471-24EA) using Aggrewell EB Formation Medium supplemented with 3 μg/ml puromycin (Life Technologies, A11138-03). TF expression was induced with doxycycline 7 days after seeding.

For flow cytometry analysis, EBs were dissociated using TrypLE Express, washed, and resuspended in FACS buffer (PBS with 10% FBS). For surface antigens, live cells were stained with fluorophore-conjugated antibodies at $1×10^7$ cells/ml for 30 minutes on ice in the dark. Stained cells were washed twice with FACS buffer, filtered into a strainer-capped tube (Falcon, 352235), and analyzed on a BD LSRII. All antibodies are listed in Supplementary Table 6. Flow cytometry data was analyzed using FlowJo 10.2.

For immunofluorescence microscopy, EBs were fixed with 4% PFA (Electron Microscopy Sciences, 15714-S) in PBS for 30 minutes at room temperature, then washed three times with PBS and kept at 4°C in PBS. Next, fixed samples were incubated with blocking solution (10% normal donkey serum, 1% BSA, 0.5% Triton X-100 in PBS) for 1 hour at room temperature. For staining, a buffer similar to the blocking buffer was used, but with reduced normal donkey serum (3%). Samples were incubated with primary antibodies at room temperature for 1 hour, subsequently washed with staining buffer twice, incubated with secondary antibodies and 1 mg/ml DAPI (Roche, 10236276001) at room temperature for 1 hour, washed once with staining buffer and then twice with PBS. EBs were finally

mounted in 1% Agarose on MatTek dishes and immersed in PBS. Stained EBs were imaged on a Zeiss LSM780 upright microscope equipped with a Zeiss Achroplan 40×/0.8 W water dipping (immersion) objective. To maximize signal to noise ratios, detector gains were kept between 600 and 900, and laser powers between 1% and 12%. Z-stacks were generated and stored in the manufacturer's format (.czi). Maximum intensity projections were exported in the ZEN blue software.

Orthogonal cell programming in cerebral organoids

Cerebral organoids were generated as previously described47 with minor modifications. To orthogonally program induced oligodendrocytes within cerebral organoids, inducible SOX9 hiPSCs and unmodified hiPSCs were dissociated with TrypLE Express (Life Technologies, 12604013), counted using an automated cell counter (Countess II, AMQAX1000, ThermoFisher Scientific) and mixed at a ratio of 1:1 in Aggrewell medium (STEMCELL Technologies, 05893). Next, the single cell suspension was transferred to Aggrewell400 plates (STEMCELL Technologies, 27945) for embryoid body formation. 600,000 cells were seeded into an Aggrewell plate containing Aggrewell medium with 10μM Y-27632 ROCK inhibitor (Millipore, 688001). The plate was spun down at 100 x *g* for 3 minutes and placed in a tissue culture incubator overnight. The next day (day 1 of the protocol), embryoid body formation was verified by brightfield microscopy and the media was changed to neural induction media (DMEM/F12, HEPES and GlutaMAX (Invitrogen, 11330-032) with N2 supplement (Gibco, A13707-01), non-essential amino acids (Gibco, 11140-050)). Half of the media was changed daily with neural induction media from days 1 to 3. On day 4, embryoid bodies were harvested by pipetting gently with a wide-bore tip to dislodge them from the Aggrewells, and were individually embedded in droplets of undiluted Matrigel (Corning, 354277). To induce TF expression for orthogonal programming, 0.5 μg/mL doxycycline was added daily into the media starting on day 4. On day 8, media was changed to neural differentiation media consisting of 1:1 DMEM/F12 containing HEPES and GlutaMAX (Invitrogen, 11330-032) and Neurobasal medium (Invitrogen, 12348-017) with non-essential amino acids (Gibco, 11140-050), N2 supplement (Gibco, A13707-01) and B27 supplement without vitamin A (Gibco, 12587-010). Media was replaced every other day. Organoids were harvested and sliced onto charged glass slides and stored at -20°C until use. For staining, samples were brought to room temperature and outlined with a wax pen. They were washed three times with MAXwash Washing Medium (ActiveMotif, 15254) to remove any remaining OCT and then blocked using MAXblock Blocking medium (ActiveMotif, 15252) for 1 hour and then washed with MAXwash Washing Medium. Primary antibodies in binding buffer (ActiveMotif, 15251) were added and allowed to stain overnight. Samples were washed three times with wash buffer and then stained for 5 hours with secondary antibodies in binding buffer. Samples were washed with wash buffer, stained with DAPI, and then mounted for imaging using VectaShield mounting media.

Statistics

All statistics including statistical tests, sample sizes and types of replicates are described in the figure legends. Exact P-values are listed in Supplementary Table 7. P-values less than 0.05 were considered significant.

Reporting Summary

Further information on research design is available in the Nature Research Reporting Summary linked to this article.

Supplementary Material

Refer to Web version on PubMed Central for supplementary material.

Acknowledgments

We thank J. Aach, M.O. Karl, R. Kalhor, N. Ostrov and H. Lee for critical feedback and the Church and Busskamp laboratories for support. We acknowledge technical support from the Harvard Biopolymers Facility, the Harvard Division of Immunology Flow Cytometry Core Facility, the Beth Israel Deaconess Medical Center Flow Cytometry Core, the Wyss Flow Cytometry and Microscopy Core, M. Ericsson and P. Coughlin at the Harvard Medical School Electron Microscopy Facility, M.T. Gianatasio at the Dana-Farber/Harvard Cancer Center Specialized Histopathology Core and Rodent Histopathology Core (both supported in part by an NCI Cancer Center Support Grant NIH 5 P30 CA06516), and Harvard Medical School Orchestra Research Computing. We also thank the TU Dresden Center for Molecular and Cellular Bioengineering (CMCB) Advanced Imaging, Deep Sequencing, Flow Cytometry and Stem Cell Engineering core facilities. We would also like to thank J. Gray's laboratory for electrophysiology support, S. Jeanty and J. Lee (Church Lab, Harvard Medical School) for the PGP1 Sendai virus hiPSC line, G. Sheynkman and W. Glindmeyer for helpful discussions, A. Jolma, K. Nitta and K. Said for technical assistance and M. Lemieux and J. McDade for their support in depositing the library to Addgene. A.H.M.N was supported by an NSERC Postgraduate Fellowship and a Peter and Carolyn Lynch Foundation Fellowship. J.E.R.A was supported by the DIGS-BB program. S.L.S. is a Shurl and Kay Curci Foundation Fellow of the Life Sciences Research Foundation. The Ellison Foundation and Institute Sponsored Research funds from the DFCI Strategic Initiative supported M.V. and D.E.H. The project was supported by the Volkswagen Foundation (Freigeist - A110720), the European Research Council (ERC-StG-678071 - ProNeurons) and by the Deutsche Forschungsgemeinschaft (SPP2127, EXC-2068-390729961 - Cluster of Excellence - Physics of Life at TU Dresden and EXC-2151-390873048 – Cluster of Excellence – ImmunoSensation^2 at the University of Bonn) to V.B. G.M.C. acknowledges funding from the National Human Genome Research Institute (NHGRI) grants P50 HG005550 "Center for Casual Variation", RM1 HG008525 "Center for Genomically Engineered Organs," the Simons Foundation for Autism Research Initiative (368485), the Blavatnik Biomedical Accelerator at Harvard University, the FunGCAT program from the Office of the Director of National Intelligence (ODNI), Intelligence Advanced Research Projects Activity (IARPA), via the Army Research Office (ARO) under Federal Award No. W911NF-17-2-0089 and research funding from R. Merkin and the Merkin Family Foundation.

Data availability

Next-generation sequencing data that supports the findings of the study are available in Gene Expression Omnibus (GEO) using accession code GSE154759.

Code availability

The code that supports the findings of this study are available from the corresponding authors upon request.

References

1. Davis RL, Weintraub H, Lassar AB. Expression of a single transfected cDNA converts fibroblasts to myoblasts. Cell. 1987; 51:987–1000. [PubMed: 3690668]
2. Takahashi K, Yamanaka S. Induction of pluripotent stem cells from mouse embryonic and adult fibroblast cultures by defined factors. Cell. 2006; 126:663–676. [PubMed: 16904174]
3. Zhang Y, et al. Rapid single-step induction of functional neurons from human pluripotent stem cells. Neuron. 2013; 78:785–798. [PubMed: 23764284]

4. Parekh U, et al. Mapping Cellular Reprogramming via Pooled Overexpression Screens with Paired Fitness and Single-Cell RNA-Sequencing Readout. Cell systems. 2018; 7:548–555. [PubMed: 30448000]
5. Tsunemoto R, et al. Diverse reprogramming codes for neuronal identity. Nature. 2018; 557:375–380. [PubMed: 29743677]
6. Pritsker M, Ford NR, Jenq HT, Lemischka IR. Genomewide gain-of-function genetic screen identifies functionally active genes in mouse embryonic stem cells. Proc Natl Acad Sci U S A. 2006; 103:6946–6951. [PubMed: 16621925]
7. Theodorou E, et al. A high throughput embryonic stem cell screen identifies Oct-2 as a bifunctional regulator of neuronal differentiation. Genes Dev. 2009; 23:575–588. [PubMed: 19270158]
8. Yamamizu K, et al. Identification of transcription factors for lineage-specific ESC differentiation. Stem cell reports. 2013; 1:545–559. [PubMed: 24371809]
9. Cahan P, et al. CellNet: network biology applied to stem cell engineering. Cell. 2014; 158:903–915. [PubMed: 25126793]
10. Rackham OJ, et al. A predictive computational framework for direct reprogramming between human cell types. Nature genetics. 2016; 48:331–335. [PubMed: 26780608]
11. D'Alessio AC, et al. A Systematic Approach to Identify Candidate Transcription Factors that Control Cell Identity. Stem cell reports. 2015; 5:763–775. [PubMed: 26603904]
12. Lambert SA, et al. The Human Transcription Factors. Cell. 2018; 175:598–599. [PubMed: 30290144]
13. Nakatake Y, et al. Generation and Profiling of 2,135 Human ESC Lines for the Systematic Analyses of Cell States Perturbed by Inducing Single Transcription Factors. Cell Rep. 2020; 31
14. Vaquerizas JM, Kummerfeld SK, Teichmann SA, Luscombe NM. A census of human transcription factors: function, expression and evolution. Nature reviews Genetics. 2009; 10:252–263.
15. Jolma A, et al. DNA-binding specificities of human transcription factors. Cell. 2013; 152:327–339. [PubMed: 23332764]
16. Seiler CY, et al. DNASU plasmid and PSI:Biology-Materials repositories: resources to accelerate biological research. Nucleic acids research. 2014; 42:D1253–1260. [PubMed: 24225319]
17. Yang X, et al. A public genome-scale lentiviral expression library of human ORFs. Nat Methods. 2011; 8:659–661. [PubMed: 21706014]
18. Wiemann S, et al. The ORFeome Collaboration: a genome-scale human ORF-clone resource. Nat Methods. 2016; 13:191–192. [PubMed: 26914201]
19. Adewumi O, et al. Characterization of human embryonic stem cell lines by the International Stem Cell Initiative. Nature biotechnology. 2007; 25:803–816.
20. Busskamp V, et al. Rapid neurogenesis through transcriptional activation in human stem cells. Mol Syst Biol. 2014; 10:760. [PubMed: 25403753]
21. Choi J, et al. A comparison of genetically matched cell lines reveals the equivalence of human iPSCs and ESCs. Nature biotechnology. 2015; 33:1173–1181.
22. Cahan P, Daley GQ. Origins and implications of pluripotent stem cell variability and heterogeneity. Nature reviews Molecular cell biology. 2013; 14:357–368. [PubMed: 23673969]
23. Chanda S, et al. Generation of induced neuronal cells by the single reprogramming factor ASCL1. Stem cell reports. 2014; 3:282–296. [PubMed: 25254342]
24. Bermingham NA, et al. Math1: an essential gene for the generation of inner ear hair cells. Science. 1999; 284:1837–1841. [PubMed: 10364557]
25. Sagal J, et al. Proneural transcription factor Atoh1 drives highly efficient differentiation of human pluripotent stem cells into dopaminergic neurons. Stem cells translational medicine. 2014; 3:888–898. [PubMed: 24904172]
26. Xue Y, et al. Synthetic mRNAs Drive Highly Efficient iPS Cell Differentiation to Dopaminergic Neurons. Stem Cells Transl Med. 2019; 8:112–123. [PubMed: 30387318]
27. Dutta A, et al. Identification of an NKX3.1-G9a-UTY transcriptional regulatory network that controls prostate differentiation. Science. 2016; 352:1576–1580. [PubMed: 27339988]

28. Mai T, et al. NKX3-1 is required for induced pluripotent stem cell reprogramming and can replace OCT4 in mouse and human iPSC induction. Nature cell biology. 2018; 20:900–908. [PubMed: 30013107]
29. Radley AH, et al. Assessment of engineered cells using CellNet and RNA-seq. Nature protocols. 2017; 12:1089–1102. [PubMed: 28448485]
30. Liang CC, Park AY, Guan JL. In vitro scratch assay: a convenient and inexpensive method for analysis of cell migration in vitro. Nature protocols. 2007; 2:329–333. [PubMed: 17406593]
31. Bell E, Ivarsson B, Merrill C. Production of a tissue-like structure by contraction of collagen lattices by human fibroblasts of different proliferative potential in vitro. Proc Natl Acad Sci U S A. 1979; 76:1274–1278. [PubMed: 286310]
32. Lee D, et al. ER71 acts downstream of BMP, Notch, and Wnt signaling in blood and vessel progenitor specification. Cell Stem Cell. 2008; 2:497–507. [PubMed: 18462699]
33. Baralle FE, Giudice J. Alternative splicing as a regulator of development and tissue identity. Nat Rev Mol Cell Biol. 2017; 18:437–451. [PubMed: 28488700]
34. Potter RF, Groom AC. Capillary diameter and geometry in cardiac and skeletal muscle studied by means of corrosion casts. Microvascular research. 1983; 25:68–84. [PubMed: 6835100]
35. Schaum N, et al. Single-cell transcriptomics of 20 mouse organs creates a Tabula Muris. Nature. 2018; 562:367–372. [PubMed: 30283141]
36. Madhavan M, et al. Induction of myelinating oligodendrocytes in human cortical spheroids. Nat Methods. 2018; 15:700–706. [PubMed: 30046099]
37. Marton RM, et al. Differentiation and maturation of oligodendrocytes in human three-dimensional neural cultures. Nature neuroscience. 2019; 22:484–491. [PubMed: 30692691]
38. Garcia-Leon JA, et al. SOX10 Single Transcription Factor-Based Fast and Efficient Generation of Oligodendrocytes from Human Pluripotent Stem Cells. Stem Cell Reports. 2018; 10:655–672. [PubMed: 29337119]
39. Ehrlich M, et al. Rapid and efficient generation of oligodendrocytes from human induced pluripotent stem cells using transcription factors. Proc Natl Acad Sci U S A. 2017; 114:E2243–e2252. [PubMed: 28246330]
40. Sarkar A, Hochedlinger K. The sox family of transcription factors: versatile regulators of stem and progenitor cell fate. Cell Stem Cell. 2013; 12:15–30. [PubMed: 23290134]
41. Bi W, Deng JM, Zhang Z, Behringer RR, de Crombrugghe B. Sox9 is required for cartilage formation. Nat Genet. 1999; 22:85–89. [PubMed: 10319868]
42. Canals I, et al. Rapid and efficient induction of functional astrocytes from human pluripotent stem cells. Nat Methods. 2018; 15:693–696. [PubMed: 30127505]
43. Khoshakhlagh P, Sivakumar A, Pace LA, Sazer DW, Moore MJ. Methods for fabrication and evaluation of a 3D microengineered model of myelinated peripheral nerve. Journal of neural engineering. 2018; 15
44. Khoshakhlagh P, Moore MJ. Photoreactive interpenetrating network of hyaluronic acid and Puramatrix as a selectively tunable scaffold for neurite growth. Acta biomaterialia. 2015; 16:23–34. [PubMed: 25617804]
45. Mohammadi S, et al. Whole-Brain In-vivo Measurements of the Axonal G-Ratio in a Group of 37 Healthy Volunteers. Front Neurosci. 2015; 9:441. [PubMed: 26640427]
46. Windrem MS, et al. Fetal and adult human oligodendrocyte progenitor cell isolates myelinate the congenitally dysmyelinated brain. Nature medicine. 2004; 10:93–97.
47. Lancaster MA, et al. Cerebral organoids model human brain development and microcephaly. Nature. 2013; 501:373–379. [PubMed: 23995685]
48. Togo S, et al. Differentiation of embryonic stem cells into fibroblast-like cells in three-dimensional type I collagen gel cultures. In vitro cellular & developmental biology Animal. 2011; 47:114–124. [PubMed: 21107747]
49. Elcheva I, et al. Direct induction of haematoendothelial programs in human pluripotent stem cells by transcriptional regulators. Nature communications. 2014; 5
50. Morita R, et al. ETS transcription factor ETV2 directly converts human fibroblasts into functional endothelial cells. Proc Natl Acad Sci U S A. 2015; 112:160–165. [PubMed: 25540418]

51. Cakir B, et al. Engineering of human brain organoids with a functional vascular-like system. Nat Methods. 2019; 16:1169–1175. [PubMed: 31591580]
52. Woltjen K, et al. piggyBac transposition reprograms fibroblasts to induced pluripotent stem cells. Nature. 2009; 458:766–770. [PubMed: 19252478]
53. Ronaldson-Bouchard K, Vunjak-Novakovic G. Organs-on-a-Chip: A Fast Track for Engineered Human Tissues in Drug Development. Cell stem cell. 2018; 22:310–324. [PubMed: 29499151]
54. Guye P, et al. Genetically engineering self-organization of human pluripotent stem cells into a liver bud-like tissue using Gata6. Nature communications. 2016; 7
55. Bagley JA, Reumann D, Bian S, Levi-Strauss J, Knoblich JA. Fused cerebral organoids model interactions between brain regions. Nat Methods. 2017; 14:743–751. [PubMed: 28504681]
56. Birey F, et al. Assembly of functionally integrated human forebrain spheroids. Nature. 2017; 545:54–59. [PubMed: 28445465]
57. Xiang Y, et al. Fusion of Regionally Specified hPSC-Derived Organoids Models Human Brain Development and Interneuron Migration. Cell stem cell. 2017; 21:383–398. [PubMed: 28757360]
58. Cederquist GY, et al. Specification of positional identity in forebrain organoids. Nature biotechnology. 2019; 37:436–444.
59. Mansour AA, et al. An in vivo model of functional and vascularized human brain organoids. Nature biotechnology. 2018; 36:432–441.
60. Rozenblatt-Rosen O, Stubbington MJT, Regev A, Teichmann SA. The Human Cell Atlas: from vision to reality. Nature. 2017; 550:451–453. [PubMed: 29072289]
61. Han X, et al. Construction of a human cell landscape at single-cell level. Nature. 2020
62. Cusanovich DA, et al. A Single-Cell Atlas of In Vivo Mammalian Chromatin Accessibility. Cell. 2018; 174:1309–1324. [PubMed: 30078704]
63. Moss J, et al. Comprehensive human cell-type methylation atlas reveals origins of circulating cell-free DNA in health and disease. Nature communications. 2018; 9
64. Gray KA, Yates B, Seal RL, Wright MW, Bruford EA. Genenames.org: the HGNC resources in 2015. Nucleic acids research. 2015; 43:D1079–1085. [PubMed: 25361968]
65. Mele M, et al. Human genomics. The human transcriptome across tissues and individuals. Science. 2015; 348:660–665. [PubMed: 25954002]
66. Church GM. The personal genome project. Mol Syst Biol. 2005; 1
67. Kutsche LK, et al. Combined Experimental and System-Level Analyses Reveal the Complex Regulatory Network of miR-124 during Human Neurogenesis. Cell systems. 2018; 7:438–452. [PubMed: 30292704]
68. Salmon P, Trono D. Production and titration of lentiviral vectors. Current protocols in human genetics. 2007
69. Dobin A, et al. STAR: ultrafast universal RNA-seq aligner. Bioinformatics (Oxford, England). 2013; 29:15–21.
70. Love MI, Huber W, Anders S. Moderated estimation of fold change and dispersion for RNA-seq data with DESeq2. Genome biology. 2014; 15:550. [PubMed: 25516281]
71. Zhang Y, et al. An RNA-sequencing transcriptome and splicing database of glia, neurons, and vascular cells of the cerebral cortex. The Journal of neuroscience : the official journal of the Society for Neuroscience. 2014; 34:11929–11947. [PubMed: 25186741]
72. Zhang J, et al. A Genome-wide Analysis of Human Pluripotent Stem Cell-Derived Endothelial Cells in 2D or 3D Culture. Stem cell reports. 2017; 8:907–918. [PubMed: 28343999]
73. Li B, Dewey CN. RSEM: accurate transcript quantification from RNA-Seq data with or without a reference genome. BMC bioinformatics. 2011; 12:323. [PubMed: 21816040]
74. Bult CJ, Blake JA, Smith CL, Kadin JA, Richardson JE. Mouse Genome Database (MGD) 2019. Nucleic acids research. 2019; 47:D801–d806. [PubMed: 30407599]
75. Anders S, Huber W. Differential expression analysis for sequence count data. Genome biology. 2010; 11
76. Leek JT. svaseq: removing batch effects and other unwanted noise from sequencing data. Nucleic acids research. 2014; 42

77. Schindelin J, et al. Fiji: an open-source platform for biological-image analysis. Nat Methods. 2012; 9:676–682. [PubMed: 22743772]

78. Ngo P, Ramalingam P, Phillips JA, Furuta GT. Collagen gel contraction assay. Methods in molecular biology (Clifton, NJ). 2006; 341:103–109.

79. Picelli S, et al. Smart-seq2 for sensitive full-length transcriptome profiling in single cells. Nat Methods. 2013; 10:1096–1098. [PubMed: 24056875]

80. Wolf FA, Angerer P, Theis FJ. SCANPY: large-scale single-cell gene expression data analysis. Genome biology. 2018; 19:15. [PubMed: 29409532]

81. Liao Y, Smyth GK, Shi W. featureCounts: an efficient general purpose program for assigning sequence reads to genomic features. Bioinformatics (Oxford, England). 2014; 30:923–930.

82. Koike N, et al. Tissue engineering: creation of long-lasting blood vessels. Nature. 2004; 428:138–139. [PubMed: 15014486]

83. Melero-Martin JM, et al. Engineering robust and functional vascular networks in vivo with human adult and cord blood-derived progenitor cells. Circulation research. 2008; 103:194–202. [PubMed: 18556575]

84. Khoshakhlagh P, et al. Development and characterization of a bioglass/chitosan composite as an injectable bone substitute. Carbohydrate polymers. 2017; 157:1261–1271. [PubMed: 27987831]

85. Khoshakhlagh P, Bowser DA, Brown JQ, Moore MJ. Comparison of visible and UVA phototoxicity in neural culture systems micropatterned with digital projection photolithography. Journal of biomedical materials research Part A. 2019; 107:134–144. [PubMed: 30358101]

86. Douvaras P, Fossati V. Generation and isolation of oligodendrocyte progenitor cells from human pluripotent stem cells. Nature protocols. 2015; 10:1143–1154. [PubMed: 26134954]

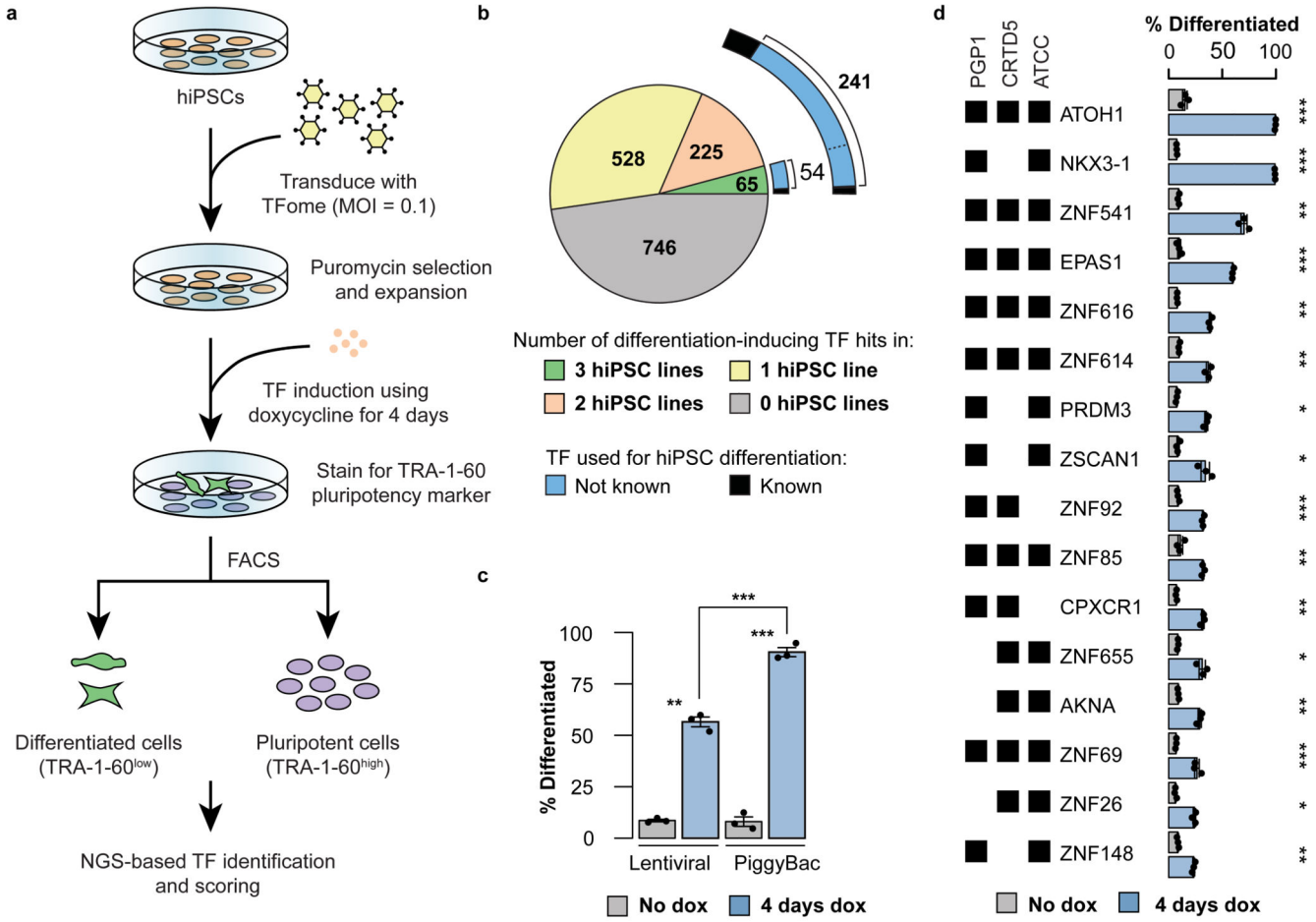

Figure 1. Creation of the Human TFome expression library and its application for cell fate engineering.

(**a**) Schematic of Human TFome screening for stem cell differentiation. MOI, multiplicity of infection = 0.1 ensures single TF integration per cell. FACS, fluorescence-activated cell sorting. NGS, next-generation sequencing. (**b**) The Human TFome screen identifies previously unreported individual TFs that induce differentiation in multiple hiPSC lines. Pie chart shows the number of differentiation-inducing TF hits in 0, 1, 2 or 3 hiPSC lines. Donut charts show the number of TF hits previously known or not known to drive differentiation upon induction. (**c**) Higher differentiation efficiency in PiggyBac-mediated versus lentiviral-mediated TF induction. Flow cytometry for differentiated cells based on loss of pluripotency markers at 4 dpi using *NEUROG1* as a canonical differentiation-inducing TF. mean±s.e.m., n = 3 biologically independent samples per group, two-sided Student's t-test. (**d**) Validation of top TF hits in individual cell lines at 4 dpi. Percentage of differentiation was calculated by loss of pluripotency markers using flow cytometry. mean±s.e.m., n = 3 biologically independent samples per group, two-sided Student's t-test. * $P < 0.05$. ** $P < 0.01$. *** $P < 0.001$. Exact P-values are provided in Supplementary Table 7.

Europe PMC Funders Author Manuscripts

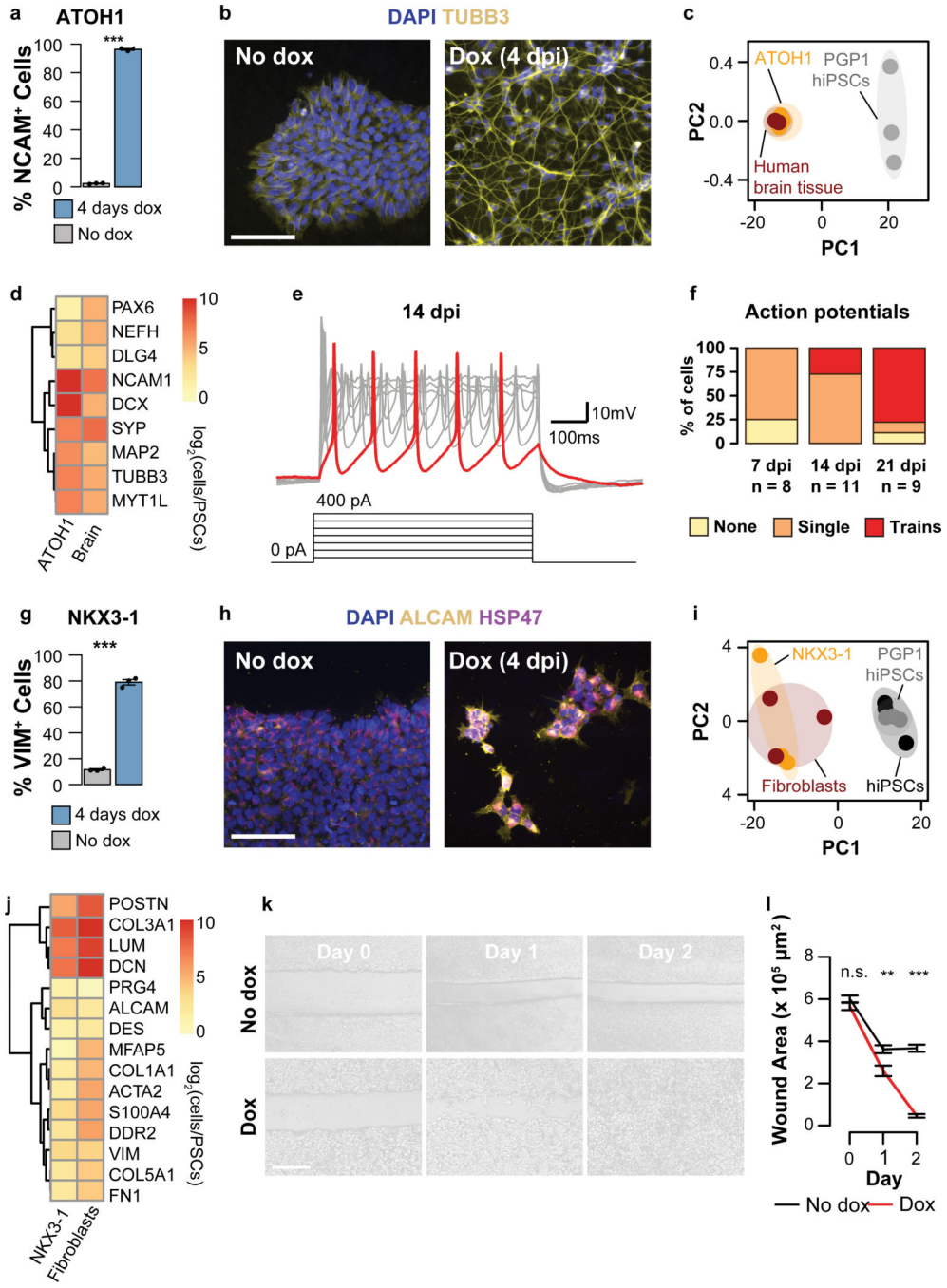

Figure 2. *ATOH1* induces neurons and *NKX3-1* induces fibroblasts in lineage-independent media.

(**a**) ATOH1 drives hiPSCs into 99±1% *NCAM*$^+$ neurons at 4 dpi. Bar plot of flow cytometry for *NCAM* neuronal marker compared to non-induced cells. mean±s.e.m., n = 3 biologically independent samples per group, two-sided Student's t-test. (**b**) *ATOH1*-induced cells exhibit neuronal morphology with *TUBB3* neuronal protein marker expression at 4 dpi compared to non-induced cells using immunofluorescent staining. Scale bar, 100 µm. Experiments were performed independently at least three times with similar results. (**c**) *ATOH1*-induced cells are transcriptomically similar to human brain tissue. Principal component (PC) analysis of

RNA-seq samples from *ATOH1*-induced cells (orange) overlap with samples from human brain tissue (red), and are distinctly separated from PGP1 hiPSCs (gray). (**d**) *ATOH1*-induced cells show similar up-regulation of neuronal markers as human brain tissue. Heatmap of neuronal gene expression profiles. (**e**) *ATOH1*-induced cells are electrophysiologically functional at 14 dpi. Electrophysiology recordings by whole-cell patch clamping after current injection. (**f**) *ATOH1*-induced cells mature over time to exhibit spontaneous trains of action potentials. Bar plots of percentage of cells having each type of action potential at 7, 14, and 21 dpi. n = number of single cells. (**g**) *NKX3-1* rapidly and efficiently induces hiPSCs into fibroblasts. Bar plot of flow cytometry for *VIM* fibroblast marker at 4 dpi compared to non-induced cells. mean±s.e.m., n = 3 biologically independent samples per group, two-sided Student's t-test. (**h**) *NKX3-1*-induced cells show fibroblast morphology with *ALCAM* and *HSP47* fibroblast protein marker expression at 4 dpi using immunofluorescent staining. Scale bar, 100 μm. Experiments were performed independently at least three times with similar results. (**i**) *NKX3-1*-induced cells are transcriptomically similar to primary fibroblasts. Principal component (PC) analysis of RNA-seq samples from *NKX3-1*-induced cells (orange) overlap with samples from primary fibroblasts (red), with a clear distance away from PGP1 hiPSCs (gray). (**j**) *NKX3-1*-induced cells show similar up-regulation of fibroblast markers as primary fibroblast based on RNA-seq analysis. Heatmap of fibroblast gene expression profiles. (**k**) *NKX3-1*-induced cells exhibit functionality in an *in vitro* wound healing assay by repairing a scratch in a confluent cell monolayer. Brightfield images of 4 dpi NKX3-1-induced cells at days 0, 1, or 2 after gap creation. Scale bar, 100μm. Experiments were performed independently at least three times with similar results. (**l**) Significant reduction in wound area by *NKX3-1*-induced cells (red), but not hiPSCs (black). Quantification of wound area in scratch assay. mean±s.e.m., n = 3 biologically independent samples per group, two-sided Student's t-test. n.s., not significant. ** $P < 0.01$. *** $P < 0.001$. Exact P-values are provided in Supplementary Table 7.

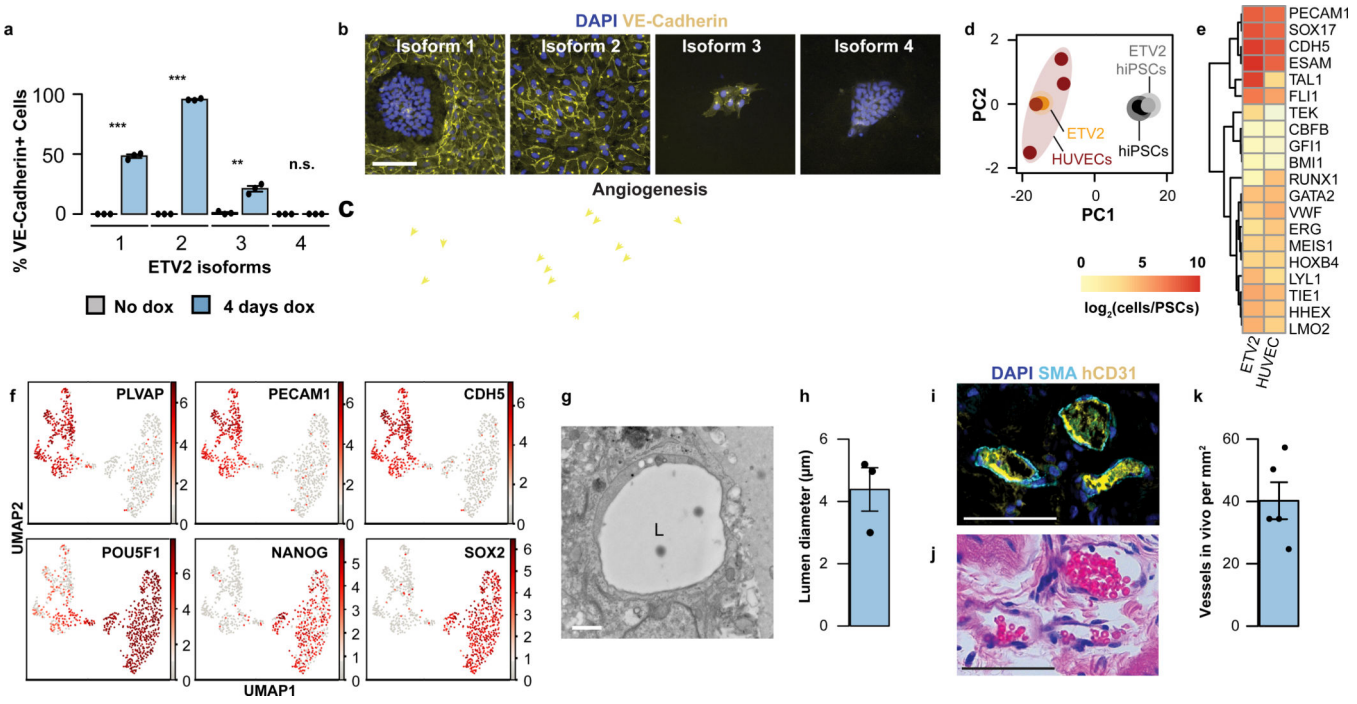

Figure 3. *ETV2* isoform 2 induces vascular endothelial–like cells that form perfusable blood vessels *in vivo*.

(**a**) *ETV2* isoform 2 induction differentiated hiPSCs into 95±0.2% VE-Cadherin^{+} (*CDH5*) vascular endothelial-like cells, which is superior to other splice-isoforms. Bar plot of flow cytometry for VE-Cadherin vascular endothelial marker at 4 dpi compared to non-induced cells for each splice-isoform. mean±s.e.m., n = 3 biologically independent samples per group, two-sided Student's t-test. (**b**) *ETV2*-isoform-2-induced cells exhibit homogeneous cobblestone endothelial morphology and VE-Cadherin protein marker expression at 4 dpi compared to other splice-isoforms and non-induced cells using immunofluorescent staining. Scale bar, 100 µm. Experiments were performed independently at least three times with similar results. (**c**) 4 dpi *ETV2*-isoform-2-induced cells form angiogenic tubes overnight, marked by arrowheads. Fluorescence imaging of *ETV2*-induced cells on thick Matrigel. Scale bar, 300µm. Experiments were performed independently at least three times with similar results. (**d**) *ETV2*-isoform-2-induced cells are transcriptomically similar to primary human umbilical cord endothelial cells (HUVECs). Principal component (PC) analysis of RNA-seq samples from *ETV2*-isoform-2-induced cells (orange) overlap with samples from HUVECs (red), and are distinctly apart from PGP1 hiPSCs (gray) and HUVEC-reference hiPSCs (black). (**e**) *ETV2*-isoform-2-induced cells show similar up-regulation of endothelial markers as HUVECs. Heatmap of endothelial gene expression profiles. (**f**) *ETV2*-isoform-2-induced cells homogeneously express vascular endothelial markers and lose pluripotency markers. Uniform Manifold Approximation and Projection (UMAP) plot of single cell RNA-seq (scRNA-seq) samples of *ETV2*-isoform-2-induced cells 4 dpi (left cluster) and hiPSCs (right cluster) showing gray (low) to red (high) for the level of gene expression of the indicated endothelial markers *PLVAP, PECAM1* and *CDH5* (VE-Cadherin), and pluripotency markers *POU5F1/OCT4, NANOG* and *SOX2*. (**g**) 4 dpi *ETV2*-isoform-2-induced cells form open lumens in an angiogenesis assay overnight. Transmission electron

Europe PMC Funders Author Manuscripts

Europe PMC Funders Author Manuscripts

microscopy (TEM) on a cross-section of tubes of angiogenic tubes. L, lumen. Scale bar, 1 μm. Experiments were performed independently at least three times with similar results. (**h**) Open lumens formed by *ETV2*-isoform-2-induced cells have diameters similar to capillaries. Quantification of lumen diameter. mean±s.e.m., n = 3 biologically independent samples. (**i**) *ETV2*-isoform-2-induced cells transplanted subcutaneously into nude mice form mature blood vessels *in vivo*. Immunofluorescent staining of a tissue section from the graft for the human-specific *CD31* (hCD31) vascular endothelial protein marker shows human endothelial cells lining open lumens, which are mature based on the surrounding SMA^+ pericytes. Scale bar, 50 μm. Experiments were performed independently at least three times with similar results. (**j**) Blood vessels formed *in vivo* by *ETV2*-isoform-2-induced cells are perfused and integrated with the host circulatory system. H&E (Hematoxylin and eosin) staining of a tissue section (serial section from panel (i)) show mouse red blood cells within the capillaries. Scale bar, 50 μm. Experiments were performed independently at least three times with similar results. (**k**) Capillaries formed *in vivo* by transplanted *ETV2*-isoform-2-induced cells have similar density to *in vivo* tissues. Quantification of number of $hCD31^+$ blood vessels. mean±s.e.m., n = 5 animals. n.s., not significant. ** $P < 0.01$. *** $P < 0.001$. Exact P-values are provided in Supplementary Table 7.

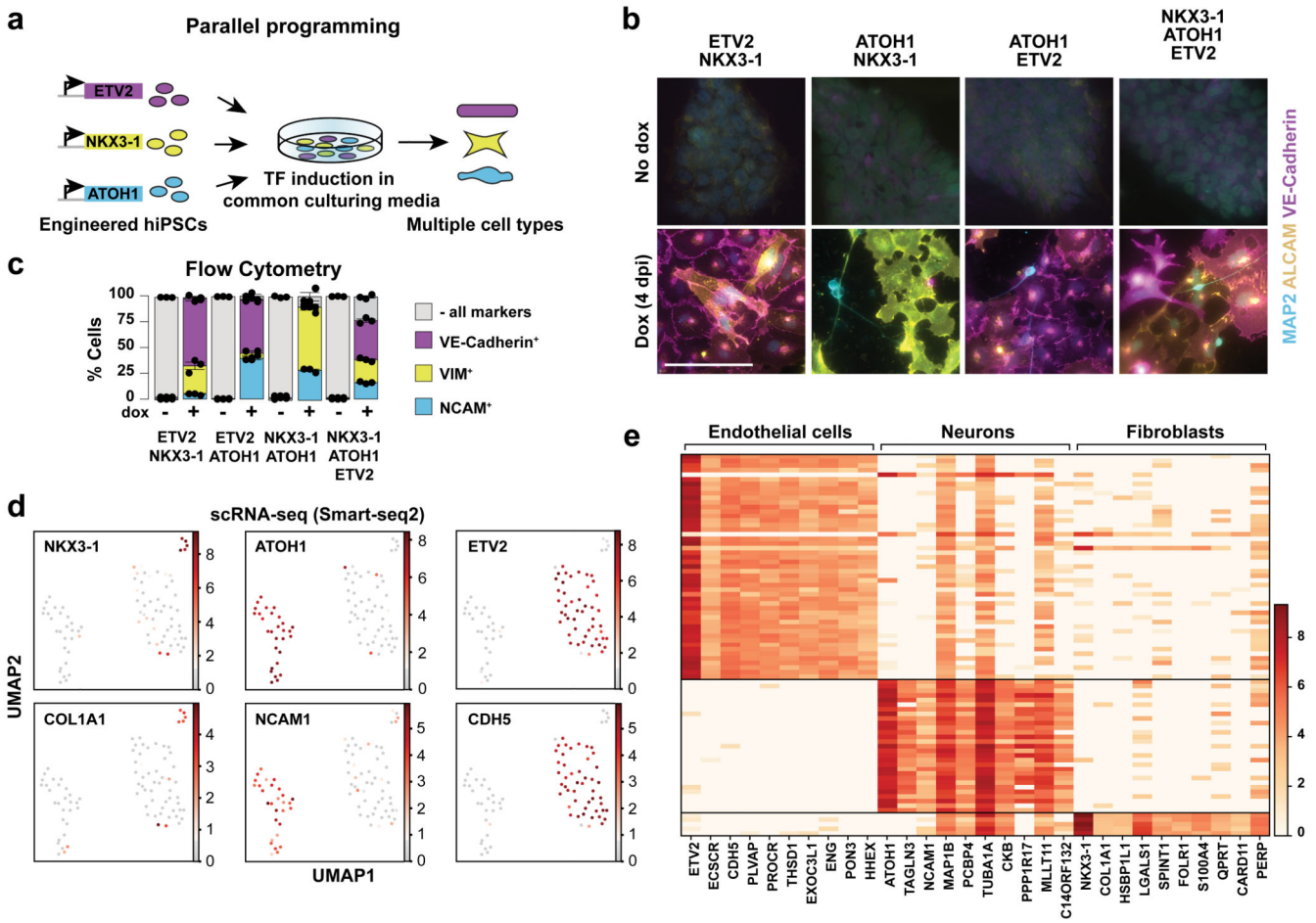

Figure 4. Parallel programming enable simultaneous differentiation of multiple cell types in the same dish.

(**a**) Schematic of parallel programming where TFs are induced and multiple cell types are produced in the same culture. (**b**) Parallel programming enables induced neurons, fibroblasts and vascular endothelial-like cells to co-differentiate in the same culture and conditions. Engineered hiPSC lines co-cultured in a pairwise fashion or altogether 4 dpi or not induced are immunofluorescently stained for the *MAP2* neuronal marker, *ALCAM* fibroblast marker and VE-Cadherin (*CDH5*) endothelial marker. Scale bar, 100 μm. Experiments were performed independently at least three times with similar results. (**c**) Parallel programming of cell lines mixed at equal ratios gives rise to co-cultures with comparable proportions for each cell type at 4 dpi. Bar plot of flow cytometry for the VE-Cadherin vascular endothelial marker, *VIM* fibroblast marker and *NCAM* neuronal marker at 4 dpi compared to non-induced cells. mean±s.e.m., n = 3 biologically independent samples per group. (**d**) Triple parallel programmed co-cultures containing *ATOH1-, ETV2-isoform-2-* and *NKX3-1-*induced cells 4 dpi homogeneously express the expected cell type-specific markers. UMAP plot of scRNA-seq using Smart-seq2 library preparation shows three distinct populations. *NKX3-1*-induced cells express the *COL1A1* fibroblast marker, *ATOH1*-induced cells express the *NCAM1* neuronal marker and *ETV2*-induced cells express the *CDH5* (VE-Cadherin) endothelial marker. Color scale from gray (low) to red (high) shows expression

Europe PMC Funders Author Manuscripts

level of the indicated genes. (**e**) Triple parallel programmed cells show distinct transcriptomic signatures that correspond to expected cell type-specific markers. Heatmap of scRNA-seq showing the top ten marker genes from each cluster as computed by Student's t-test. Single cells as rows and genes as columns.

Europe PMC Funders Author Manuscripts

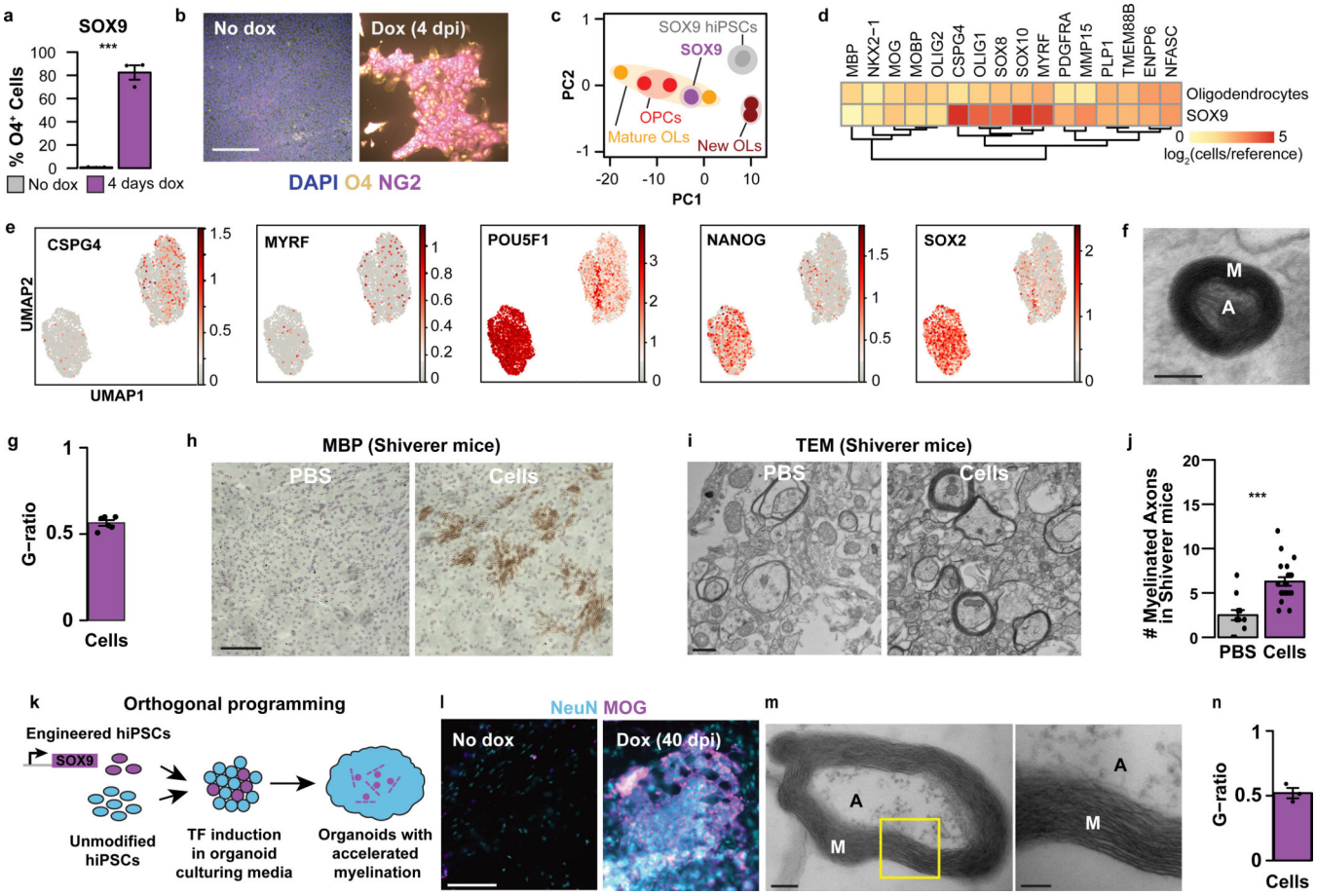

Figure 5. *SOX9* induces oligodendrocytes that engraft and form compact myelin *in vivo* and in cerebral organoids.

(**a**) *SOX9* rapidly and efficiently programs hiPSCs into induced oligodendrocytes at 4 dpi. Bar plot of flow cytometry for O4 oligodendrocyte marker compared to non-induced cells. mean±s.e.m., n = 3 biologically independent samples per group, two-sided Student's t-test. (**b**) *SOX9*-induced cells exhibit O4 and NG2 oligodendrocyte protein marker expression at 4 dpi compared to non-induced cells using immunofluorescent staining. Scale bar, 100 μm. Experiments were performed independently at least three times with similar results. (**c**) *SOX9*-induced cells are transcriptomically similar to primary oligodendrocytes. Principal component (PC) analysis of RNA-seq samples from SOX9-induced cells (purple) overlap with samples from primary mature oligodendrocytes (OL; orange), with similarity to oligodendrocyte progenitor cells (OPCs; red), and are distinctly separated from newly formed oligodendrocytes (OLs; brown) and PGP1 hiPSCs (gray). (**d**) *SOX9*-induced cells show similar up-regulation of oligodendrocyte markers as primary oligodendrocytes. Heatmap of oligodendrocyte gene expression profiles. (**e**) *SOX9*-induced cells form a homogeneous cluster that expresses oligodendrocyte markers and lose pluripotency markers. UMAP plot of scRNA-seq samples of SOX9-induced cells 4 dpi (right cluster) and hiPSCs (left cluster) showing gray (low) to red (high) for the level of gene expression of the indicated oligodendrocyte markers *CSPG4* (NG2) and *MYRF*, and pluripotency markers *POU5F1/OCT4, NANOG* and *SOX2*. (**f**) Parallel programming of *SOX9*-induced

Europe PMC Funders Author Manuscripts

oligodendrocytes and hiPSC-derived inducible neurons produces synthetic oligo-neuronal co-cultures that form compact myelin *in vitro*. TEM on a cross-section of the oligo-neuronal co-culture in the photo-micropatterned microchannels. M, myelin. A, axon. Scale bar, 100 nm. Experiments were performed independently at least three times with similar results. (**g**) Quantification of G-ratio for myelin compaction is within the physiological range. mean ±s.e.m., n = 6 independent samples. (**h**) Transplanted *SOX9*-induced cells engraft and express *MBP* in Shiverer (*MBP* knock-out) mice at 2.5 months. Immunofluorescent staining of a brain tissue section for the *MBP* myelin marker after PBS injection or SOX9-induced cell transplantation into Shiverer mice. PBS, phosphate buffered saline. Scale bar, 200 μm. Experiments were performed independently at least three times with similar results. (**i**) Transplanted *SOX9*-induced cells form compact myelin in Shiverer mice. TEM of a cross-section from PBS-injected or SOX9-induced cell transplantation into Shiverer mice. Scale bar, 600 nm. Experiments were performed independently at least three times with similar results. (**j**) Shiverer mice with transplanted *SOX9*-induced cells have significantly more myelinated axons than PBS-injected animals. Quantification of the number of myelinated axons from PBS-injected or SOX9-induced cell transplantation into Shiverer mice. mean ±s.e.m., n = 12 micrographs taken at distinct locations derived from two PBS-injected animals and n = 21 micrographs taken at distinct locations derived from three animals with cell transplantation, two-sided Student's t-test. (**k**) Schematic of orthogonal programming where engineered hiPSCs for TF-inducible differentiation are incorporated at the genesis of developmentally inspired cerebral organoids to synthetically accelerate myelination. (**l**) Orthogonal programming of inducible *SOX9* cells within cerebral organoids accelerated expression of the *MOG* myelin marker. Immunofluorescent staining of a cerebral organoid section for *MOG* myelin marker and NeuN neuronal marker in orthogonally induced versus non-induced organoids. Scale bar, 100μm. Experiments were performed independently at least three times with similar results. (**m**) *SOX9* orthogonally programmed organoids for compact myelin. TEM of myelin in a cerebral organoid. Yellow region magnified on right. M: myelin, A: axon. Scale bar, 200 nm. Inset scale bar, 100 nm. Experiments were performed independently at least three times with similar results. (**n**) Quantification of G-ratio for myelin compaction in cerebral organoids shows physiological resemblance. mean ±s.e.m., n = 3 biologically independent samples. *** $P < 0.001$. Exact P-values are provided in Supplementary Table 7.